DISPLACEMENT OF DRILLING MUD DURING PRIMARY CEMENTING IN NEAR VERTICAL OIL WELLS

by

SHALU SOOD

B.Tech (Chemical Engineering), Punjab Technical University 2001

A THESIS SUBMITTED IN PARTIAL FULFILLMENT OF

THE REQUIREMENTS FOR THE DEGREE OF

MASTER OF APPLIED SCIENCE

in

THE FACULTY OF GRADUATE STUDIES

DEPARTMENT OF CHEMICAL AND BIOLOGICAL ENGINEERING

We accept this thesis as conforming
to the required standard

THE UNIVERSITY OF BRITISH COLUMBIA

March 2004

Library Authorization

SHALU SOOD
Name of Author *(please print)*

29/03/2004
Date (dd/mm/yyyy)

Title of Thesis: DISPLACEMENT OF DRILLING MUD DURING PRIMARY CEMENTING IN NEAR-VERTICAL OIL WELLS.

Degree: M.A.Sc. Year: 2004

Department of CHEMICAL AND BIOLOGICAL ENGINEERING
The University of British Columbia
Vancouver, BC Canada

Abstract

In this thesis, we consider the physical problem that stems from the industrial process of oil well cementing during the well's construction. The laminar flow of non-Newtonian fluids in an eccentric annuli has been the subject of many investigations. The work presented here is part of a combined theoretical-experimental approach to the problem of non-Newtonian displacement.

An annular flow loop is constructed so that controlled experiments can be performed on fluid displacements. We conduct a series of experiments using two different carbopol solutions. The drilling muds are non-Newtonian in nature and exhibit a yield stress, we investigate the effects of primary factors, i.e. eccentricity, inclination, density contrast, pH and concentration of carbopol solutions on the displacement of two non- Newtonian fluids in an eccentric annulus.

From the experimental results, we classify the regimes of stable and unsteady displacements qualitatively. We report a new phenomenon of flow bypass occurring for concentric cases. We compare our experimental results with a simplified model which allows for a prediction of the displacement flow type.

The lubrication model is not in good agreement with the experimental results.

Table of Contents

List of Tables

List of Figures

Acknowledgments

This research has been supported by Schlumberger Oilfield Services and by NSERC Canada through project 245434.

I would like to thank my supervisors, Dr. Mark Martinez and Dr. Ian Frigaard for their endless patience, guidance and encouragement throughout. Many thanks to Dr. Cherif Nouar for his invaluable suggestions.

I would like to thank Dr. Sheldon Duff for helping me out at the start of my Graduate Career. Your help is gratefully acknowledged.

Many thanks to Andrew, Anthony, Cassie, Sina and Miguel for helping me out at different stages of my project and for never saying "no" to any help that I required over the course of project.

I wish to thank my family for giving me an opportunity to pursue my dreams.

Finally, I would like to thank my Laptop for not crashing on me during the crucial times.

Chapter 1
Introduction

1.1 Process description

In construction of oil and gas wells it is necessary to cement a series of steel casings into the well as the depth increases. These cemented steel tubes serve a dual purpose:

1. The cemented casings serve to support the well bore, preventing collapse.
2. The cement provides a hydraulic seal on the outside of the steel casing, between casing and rock formation, along the length of the well. This is necessary in order to isolate the different fluid-bearing zones of the rock formation from one another and from the surface.

The process by which this is commonly achieved is called primary cementing. The main purpose of the primary cementing job is to remove the drilling mud from the wellbore and to completely fill the wellbore with the cement slurry. The primary cementing process, (see e.g. [1, 3, 9, 12, 17]), proceeds as follows (Figure 1.1): A new section of well is drilled. The drill pipe is removed from the wellbore, leaving the drilling mud inside the wellbore. A section of steel casing is inserted in the wellbore, leaving a gap between the outside of the tube and the inside of the wellbore i.e. the annulus. Centralizers are also fitted to the outside of the casing, to prevent the heavy steel casing from slumping to the narrow side of the wellbore. It is very common that the annular gap is eccentric, especially in inclined wellbores. Once the tube is in place, with drilling mud on the inside and outside, a sequence of fluids is pumped down the inside of the tubing, reaching the bottom of the well and coming back up through the annular gap. Typically, a wash or spacer fluid is pumped first, displacing the drilling mud left over, both on the inside of the tubing and outside in the annulus, followed by one or more cement slurries.

Spacers have designed density and rheological properties and minimize the contact between the cement slurry and the drilling mud. For effective mud removal, the density of the spacer should be higher than that of the drilling mud but lower than that of the cement slurry. Drilling mud follows the final cement slurry pumped and circulation is stopped with a few meters of cement left at the bottom inside the casing. The cement is then allowed to set. The final part of the cement inside the casing is drilled out as the well proceeds. Some typical parameters, [1, 9, 12], for a primary cementing job are shown in Table 1.1.

Characteristics	Value
Length of cemented section	300–1000m
Well inner diameter	10–50 cm
Time taken for the cement to set	6–18 hrs
Inclination of the well	0–100 degrees
Annular gap	$\approx$ 2 cm

Table 1.1: Typical characteristics of a cementing job.

1.2 Problems encountered with primary cementing

A successful cement job results in removal of mud and spacer fluid from the annulus by the cement slurry. Unfortunately, many problems may arise during the primary cementing process. The most important from the perspective of this thesis are those associated with a failure to completely remove the drilling mud.

The problems related to mud removal are of two principal category:

1. The residual mud could mix with the cement, causing contamination and preventing hardening of the cement.

2. The mud may remain unmixed but may not be fully removed from the annulus during

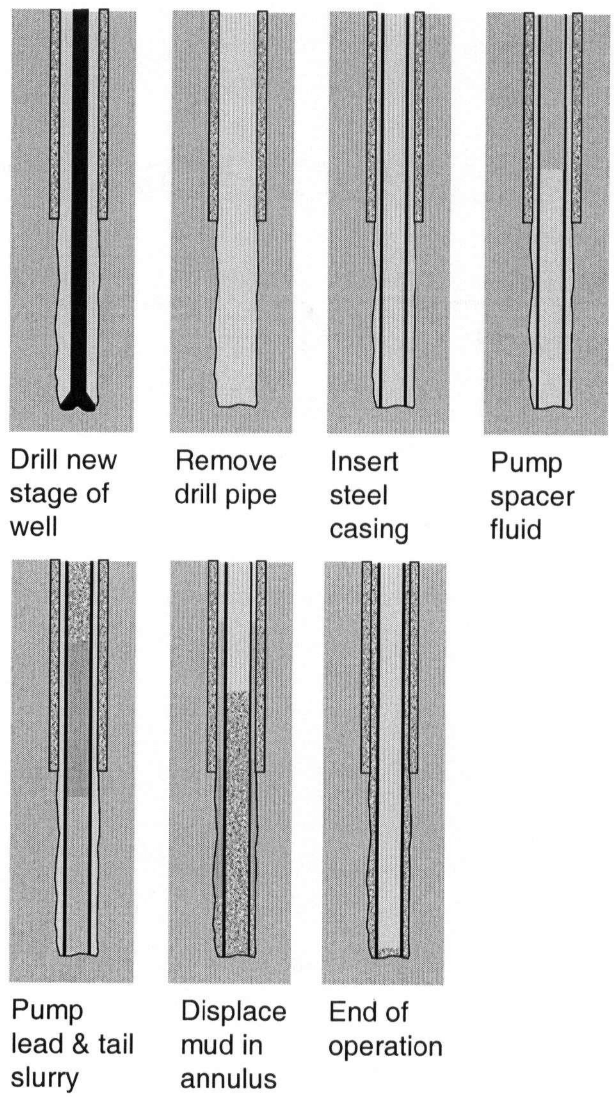

Figure 1.1: Schematic of primary cementing operation.

the displacement process, remaining in the annular gap between the casing and the hole.

This could result in the formation of a mud channel on the narrow side of the annulus (Figure 1.2). The possibility of a mud channel forming on the narrow side of the annulus was first identified and examined, [2], using hydraulic approach. The hydraulic approach considers the flow of a single fluid along a duct and makes predictions based on comparisons of the hydraulic characteristics of these flows for the different fluids being pumped, e.g. is there a flow, comparing frictional pressures and flow rates. It was observed that the tendency of the cement to bypass mud is a function of the geometry of the annulus, the density and flow properties of the mud and cement and the rate of flow. The approximate guidelines, [2], for effective mud removal are :

1. The cement slurry must be thicker than the mud to prevent bypassing in an eccentric annulus unless displacement of mud is aided by motion of the casing or buoyant forces.
2. The yield strength of the cement should be maintained greater than the yield strength of the mud multiplied by the maximum distance from the casing to the wall of the borehole and divided by the minimum distance.

The reason that a channel forms is related to the annulus being eccentric, (i.e. not concentric) and to the fluids having a yield stress. A fluid with yield stress will not move unless a critical yield stress is exceeded. In cementing, where the annulus is eccentric, the fluids move preferentially on the wider side of the annulus, since a lower frictional pressure is required. Even if the mud does not channel is it natural for the fluids to move faster on the wide side of an eccentric annulus than on the narrow side since there is less friction. This difference in velocity can result in the onset of instabilities, [16], that occur when a single yield stress fluid is displaced by itself. The instabilities also arise in case of two yield stress fluids, [15, 16], when a fluid is pushed by a less viscous one. This takes the form of fingering (Figure 1.2). Much work has been focused on these instabilities.

Thus, to avoid mud channeling and the instabilities, the ideal situation is that in which a steady and stable interface between the two fluids advances along the annulus at the mean pumping

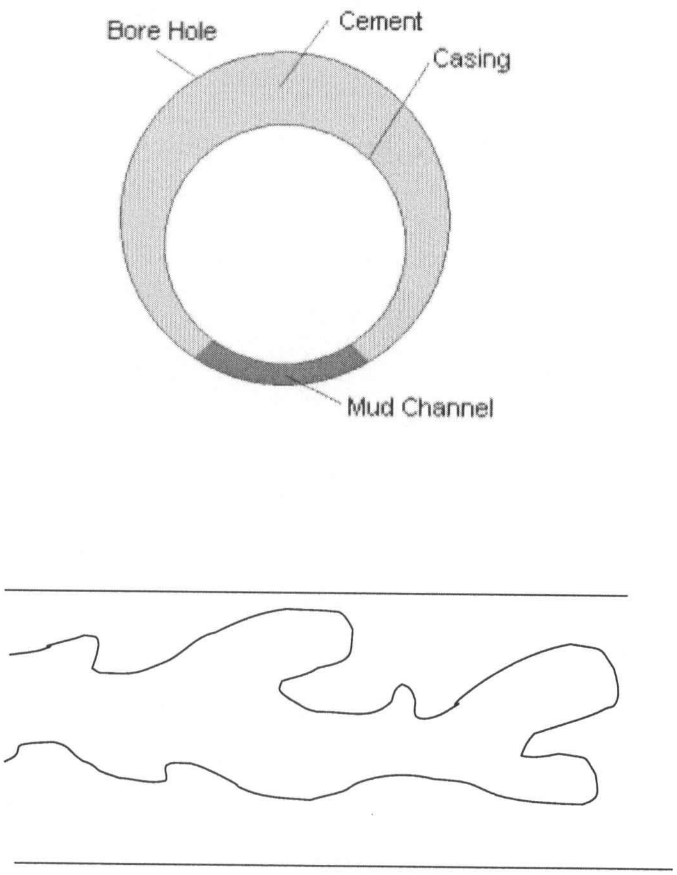

Figure 1.2: Mud channel and finger formation.

speed. Poor mud removal in an eccentric annulus remains an important industrial problem to be studied and a better comprehension of the mechanisms of the removal of drilling muds by the cement is therefore essential.

1.3 Non-Newtonian fluids

1.3.1 Property of the drilling fluids

A sequence of specially prepared fluids (washes, spacers and cement slurries), is pumped into the well. To facilitate the mud removal process it is possible to modify the rheologies and densities of these fluids within limits. The rheology of the fluids depends on many factors, [1, 4]:

1. The viscosity of the liquid phase.
2. The volume of solid particles.
3. Volume of dispersed fluids (emulsions)
4. The form of the solid particles.

Generally, washes help to liquify drilling muds. These fluids are of low density, essentially water. Spacers are used to separate drilling mud from the cement slurries in a manner to avoid all contamination. They have a higher density than the washes. Their compositions and rheological characteristics are intermediary between that of mud and cement.

Fluids are described as Newtonian or non-Newtonian depending on their response to shearing. The shear stress of a Newtonian fluid is proportional to the shear rate. Most drilling muds are non-Newtonian fluids, with viscosity decreasing as shear rate increases. In general, these fluids are inelastic shear thinning fluids with a yield stress. There are various models which describe the behavior of non - Newtonian fluids. In the industry, these fluids are often modeled as incompressible Bingham plastic, Power-Law or Herschel-Bulkley fluids (Figure 1.3). Bingham plastic fluids show a linear shear-stress, shear-rate behavior after an initial shear-stress threshold has been reached. Power law fluids are shear thinning in nature. Herschel-Bulkley

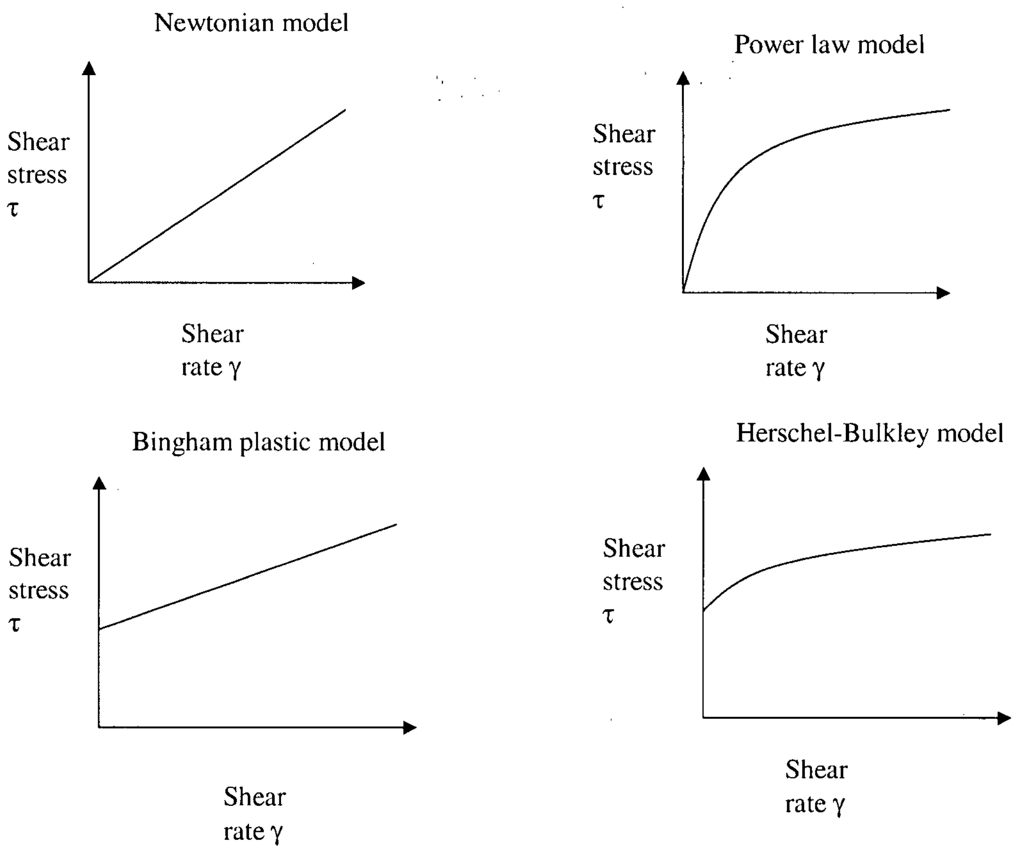

Figure 1.3: Stress vs strain rate behavior for various single non-Newtonian fluids.

fluids require a certain minimum stress to initiate the flow, but decrease stress with increasing shear. These can be described mathematically as follows:

$$\tau = \tau_y + \kappa \cdot \dot{\gamma}^n \tag{1.1}$$

where τ is the shear stress, τ_y is the yield stress, κ is the consistency, $\dot{\gamma}$ is the shear rate and n is the power law index of the fluid.

This law represents an idealized model for the behavior of the fluids. The two ways in which the fluids diverge from the ideal behavior are: thixotropy and viscoelasticity. Thixotropy is the characteristic of the drilling mud to form a gelled structure over time when not subject to shearing and then to liquify when agitated. The viscosity of such a fluid changes with time under constant shear rate until reaching equilibrium. Viscoelasticity is an intermediary behavior between a solid and a viscous fluid. It is characterized by coefficient of elasticity and by a viscosity.

Thus, we are led to the design problem of how best to displace one non-Newtonian fluid with another, along an eccentric annulus.

1.4 Industrial practices for mud removal

The focus of much industrial research into primary cementing has been to understand how different fluid rheologies and densities affect the displacement of the mud in the eccentric annulus, [1, 2, 4, 5, 6, 7, 8].

In selection of cement or mud spacers to effect good mud displacement, six criteria should be considered:

1. Spacer rheology and pump rates.
2. Mud/cement/spacer compatibility.
3. Spacer water-wetting characteristics.
4. Spacer density and solids-suspending characteristics.

5. Contact time.

Hydraulic reasoning has been used in the majority of the industrial literature on the subject, leading to several systems of design rules, [5, 6, 7] for a successful cementing job. In general, these rule sets state as follows:

1. Flow rate must be sufficiently high to avoid a mud channel on the narrow side of the annulus.

2. There should be a hierarchy of the fluid rheologies pumped (i.e. each fluid should generate a higher frictional pressure than its predecessor).

3. There should be a hierarchy of the fluid densities (i.e. each fluid should be heavier than its predecessor).

4. The gel strength of the displaced fluid mud be broken during mud circulation, prior to displacement.

5. The yield stress of each fluid must be overcome on the narrow side of the annulus: achieved when the wall shear stress generated by hydrostatic pressure gradient and frictional pressure gradient exceeds yield stress of displaced fluid.

6. The interface on the narrow side of the annulus has to move atleast as fast on the wide side to avoid channeling.

Another such system of rules currently used in well construction is the WELLCLEAN system, developed by Schlumberger, [8, 9, 1]. These rules state:

1. There should be a density hierarchy of 10 % between each pair of displacing and displaced fluids.

2. There should be a frictional pressure hierarchy of 20% between each pair of displacing and displaced fluids.

3. The frictional pressure in the displacing fluid should be sufficient to exceed the yield stress of the displaced fluid on the narrow side plus the difference in axial static density

gradients. This corresponds to the minimum pressure gradient required to ensure mobile mud.

4. In an eccentric annulus, the flow of the displacing fluid on the wide side should not be faster than the displaced fluid on the narrow side. This is called the differential velocity criterion.

These rules depend on stable laminar displacement.

WELLCLEAN is a practically sensible system for confirming that mud removal will be efficient, when the assumptions are valid.

1.5 Current state of knowledge

Extensive work has been done in the primary cementing area previously. The experimental studies undertaken, [4], investigate the importance of displacement factors namely; the condition of drilling fluid, rheological differences, flow rate, fluid volume and density differences.

1. It is observed that in the experimental studies, displacement is not appreciably affected by the amount of fluids pumped at lower flow rates. Once, the cement determines a flow path, it continues to follow the path with little or no deviation.

2. It is observed that increasing the density difference between the fluid mud and cement by as much as $360kg/m^3$ does not improve the overall displacement.

3. Pumping high yield stress cement at low flow rates is not an effective method of mud displacement.

In another combined experimental and theoretical investigation of laminar displacement in an inclined annulus, [19], it is observed:

1. Inclination reduces the displacement process by decreasing the gravitational effects. This can be compensated for by optimizing the pump rate and fluid rheologies.

2. There is a strong interaction between the density difference and the pump rate which can reduce the instabilities. However small pockets of the displaced fluid may be entrapped in the narrow side.

3. Good spacer design is essential in the efficient removal of mud by the spacer and cement.

In another experimental investigation to determine the importance of displacement factors, [3], it is observed:

1. In the test sections simulating displacement process, 100 percent displacement is never achieved.

2. In a narrow annulus, slightest eccentricity is enough to allow a channel of mud to be bypassed. This is caused by the resulting nonuniform pressure distribution in the annulus.

3. High cement flow rates appear to favorably influence the mud displacement process.

4. Within the realistic range of cement and mud properties studied, the rheological difference did not have measurable effect on the displacement process.

1.6 Cementing displacement research at UBC

More recently, a research program was started at the University Of British Columbia supported by Schlumberger and NSERC, in order to investigate primary cementing displacements, both experimentally and through modeling and simulation. Computational requirements for simulating 3-D flow over the scale of the wellbore are prohibitive and only an annular cross-section of the domain is usually considered. It reduces the problem to two dimensions. The general idea is based in considering bulk fluid motions by averaging across the annular ducts. This is similar to computing flows as in classical Hele-Shaw displacement studies, [15, 16]. A simplified model for evolution of the interface using methods applied to lubrication and thin-film flows is derived, [13]. The problem is reduced to a 1-D model. The work is based on [12]. The simplified model presented in [13] gives a criterion for the type of fluid displacement occurring without actually simulating the entire flow. Essentially, the displaced fluid is assumed to be elongated on the wide side of the annulus. By looking at whether the interface elongates or not, it is concluded whether or not the given situation would result in an stable or unsteady displacement. An Annular flow loop is constructed so that experiments can be performed on fluid displacements in an eccentric annulus using fluids with similar rheologies to those used in primary cementing, [14]. Data from these experimental observations are compared with model predictions and used to gauge the validity of assumptions made in the modeling process.

1.7 Outline of the thesis

In this thesis, we focus our attention on understanding the problems related to primary cementing and predicting steady state displacements by experimentally investigating the effects of various parameters, such as inclination and eccentricity of the flow loop. Rheology, density and flow rates of the fluids are also taken into effect. In chapter 2, we describe the design and construction of the annular flow loop. We also give a detailed description of the fluid preparation and characterization. The experimental procedure and experimental plan are discussed in detail. In chapter 3, we describe the mathematical model. In chapter 4 we present our experimental results. In addition, we compare the experimental results with the mathematical model. Finally, in chapter 5, we analyze our experimental data and end with a discussion. Recommendations for future work are also given.

Chapter 2
Procedures and Experimental System

2.1 Annular Flow Loop

2.1.1 Objectives

Since Primary Cementing occurs many hundreds of meters below the surface it is impossible to observe the displacement behavior of the different fluids in real situations. Different approaches like modeling, CFD simulation and experimentation are used to understand and improve the process.

The annular flow loop is constructed so that controlled experiments can be performed on fluid displacements in an eccentric annulus using fluids with similar rheologies to those used in primary cementing. The experimental parameters and results can both be observed and measured. Data from these observations will be compared with model predictions and used to gauge the validity of assumptions made in the modeling process. Additionally, new phenomena might be observed which are not predicted by the modeling.

Eventually, experimental and model results will be combined and will be used to specify the conditions under which cementing displacements will be effective.

2.1.2 Design Requirements

To simulate the fluid displacement during the primary cementing the annular flow loop must meet the following requirements:

1. The center tube of the annulus must be moveable on one axis to allow change of

eccentricity.

2. The flow loop must be usable in various inclinations including horizontal and vertical positions.

3. The interface between the two fluids should be visible so it can be recorded easily on the video.

4. The displacing fluid must be supplied at laminar flow rates.

2.1.3 Annulus Structure

Overall Structural Design

Since the annulus design requires a way to raise and lower the annulus to different angles, a way has to be devised to achieve this. An electric winch is selected to raise and lower the annulus. A pair of extendable legs was designed to support the raised end of the annulus in order to increase its stability during the operation (Figure 2.1). The winch raises the annulus, the legs extend and then the winch lowers the annulus onto the legs. The other end of the annulus is mounted to a stand at about 1.5 m above the ground. The length of the annulus is 6.1 meters(20 ft). The overall size of the annulus is limited by the size of the building it will be built in. The height of the building limits the annulus to about 6 meters in length. A length of 6.1 meters is chosen as a lot of material is sold in 6.1 meter lengths.

Annulus tubes

Outer Tube

The outer tube must be made of a clear, transparent material so that the fluid interface can be observed. Plexiglas was chosen to provide optical clarity and better tolerance. The Plexiglas tubing was available in the required 0.0889 m inner diameter with a 0.003175 m wall thickness for an outer diameter of 0.0889 m. The tubing was manufactured in 6 ft (1.83 m) lengths. Four tubes were necessary to reach the design length of 6.1 m.

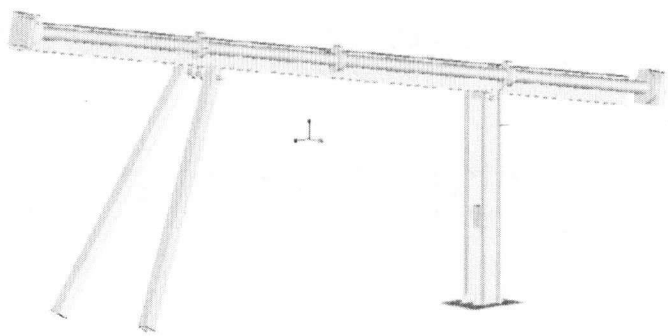

Figure 2.1: Annulus design structure

Inner Tube

Unlike the outer tube, stiffness is considered a key requirement for the inner tube. Stainless steel is chosen because it is available with a 180 grit standard finish. Improved finish is desirable for improved fluid flow around the tube. The inner tube is supported in three places with the help of middle support structures along its lengths in addition to being supported at the ends. The end blocks are made of aluminum. The length in between supports is approximately 1.53 m.

Annulus End Supports

The design of the supports at each end of the annulus is copied from a similar annulus constructed by Schlumberger in Clamart, France . The ends are made of aluminum instead of Plexiglas, as in the Schlumberger design, for ease of machining and cost. The end piece must move the inner tube relative to the outer tube on one axis. To accomplish this, the inner tube is mounted to a sliding block. This block contains linear ball bearings, and slides on a pair of shafts. The outer tube is mounted to the stationary part of the end piece. The stationary part also holds the ends of the shafts on which the sliding block moves. A micrometer head on one side of the block and a bolt on the other side control the sliding of the inner block. The micrometer head accurately positions the block, and the bolt ensures the block is pushed up

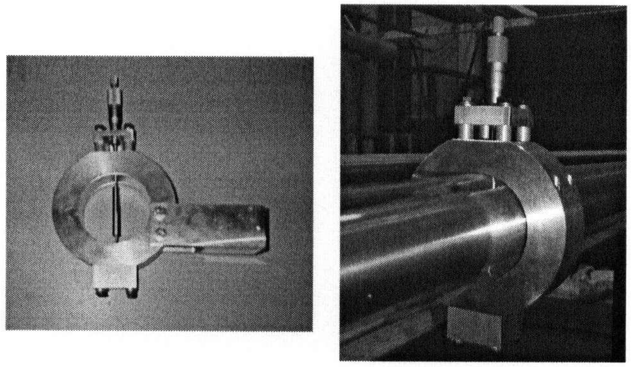

Figure 2.2: Middle support structures.

against the micrometer head. The Plexiglas tube is sealed to the stationary block using an O-ring. The stainless steel tube is also sealed to the sliding block with an O-ring.

Annulus Middle Support Structures

Three middle support structures (Figure 2.2) are constructed and placed along the length of the annulus. The supports serve two purposes. They join the different segments of the outer Plexiglas tube, and they support the inner stainless steel tube, limiting its deflection.

A two-pin system is chosen to support the inner tube at various locations along its length. The two-pin system ensures that the tube does not fall out from between the pins. The two pins are mounted parallel to the axis of desired motion. The end of each pin entered a socket on each end of a rod welded into the center tube. The surface of each socket is mounted flush with the surface of each tube. Each pin fit in its socket tightly with a slight clearance fit. This prevents the inner tube from moving perpendicular to the pins. To adjust the position of the tube along the one axis of motion, one pin is moved in further, while the other one is backed out. A micrometer head is used to control the motion of one pin while a bolt moves the pin on the other end. The micrometer head is used to adjust the inner tube position, with bolt ensuring the tube is located firmly against the micrometer head controlled pin.

The outer Plexiglas tube is supported in three locations by the clamps that house the pin supports for the inner tube.

Annulus Support

The annulus tubes are mounted to a stiff support to insure a minimum deflection over the length of the annulus. A 4 by 8 inch aluminum I-beam is chosen for the support as it is ready made requiring no construction or custom fabrication, is the stiffest shape available beam, and is significantly lighter than a steel beam.

Winch

An electric winch is used to raise and lower the annulus in a controlled fashion, and holds the annulus up as the legs are extended. The winch selected is a Super winch SAC 1000. It includes a full load mechanical brake that holds the annulus stationary. The winch runs on 120V AC power that is available in the lab. A safety switch prevents the winch from continuing to pull once the annulus is in vertical position. The switch is built into the main base stand, and is triggered when the annulus reaches a vertical position.

Stands

The main pivot for the annulus is located on a base stand approximately 1.5 m tall (Figure 2.1). This pivot is located off the ground so that a length of the annulus can be located on each side of the pivot. The shorter side swings down as the rest rotates up. The serves to reduce the winch load. The pivot is also located on this stand so the annulus sits about at eye level when in the horizontal position.

A second stand is built to hold the other end of the annulus when it is a horizontal position. Two bolts are threaded into the top of the stand to allow the stand height to adjust to ensure that the annulus is horizontal.

Extendable Legs

A pair of extendable legs support the annular flow loop when it is operated in positions other than horizontal (Figure 2.1). Each leg consists of a square aluminum tube mounted inside another square aluminum tube. Plastic pads are mounted to the inner tube to take up the space between the two tubes. To extend the leg, the inner tube is slid out of the outer tube. A pair of bolts is placed through the tubes to hold the leg in its extended position. Both legs are mounted to the I-beam via a shaft and bearings.

2.1.4 Pump System

The viscoplastic fluid used in our experiments is Carbopol (Section 2.2.1). Only certain types of pumps are compatible with Carbopol solutions. Many types of pumps cut the polymer chains in the solutions as it is pumped, altering the fluid properties. A minimum pressure gradient is necessary to overcome the yield stress of the fluid. Below this pressure gradient, the fluid will not flow.

The pump system consists of a progressive cavity pump hooked up to a variable speed motor yielding various flow rates.

Pump

The apparatus uses a progressive, pulsation free cavity pump, which is crucial for the fluid flow to have no physical disturbance. A variable speed setup is used to control the actual flow rate. The Eagle EP56-CSQM provides a suitable range of flow rates for the annulus. This model provides a maximum flow rate of approximately 57 liters per minute at 1150rpm, the maximum speed recommended by the manufacturer.

2.1.5 Camera System

Three cameras are mounted on one side of the annulus so that the experiments can be recorded regardless of the annulus position.

The cameras are mounted equidistantly on one side of the annulus. The test is started and the interface is formed between the two fluids. The interface begins to move along the length of the annulus. The position of the interface is observed and recorded at three different positions, where three cameras are placed by switching between the three cameras using a

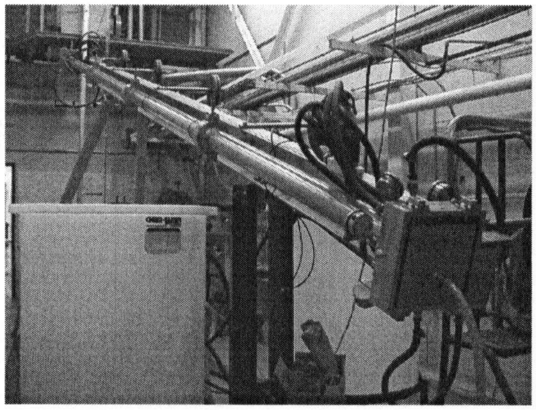

Figure 2.3: Flow loop.

remote control and the test is recorded with the help of a VCR.

The complete structure of the flow loop is shown (Figure 2.3). More information on the design and construction of the flow loop can be found in [14].

2.2 Fluid Preparation and Characterization

In this section we will discuss the technique of measuring rheologies, choice and the description of the fluids.

2.2.1 Carbopol

For the last 50 years or so, Carbopol (Figure 2.4), B.F. Goodrich commercial polymeric thickener has been one of the most widely used thickening and gelling agents for commercial aqueous products in the personal, homecare and pharmaceutical areas. Most Carbopol-type polymers (also called carbomer resins) are high molecular-weight copolymers of acrylic acid and are heavily cross-linked (intra-molecularly) with a polyalkenyl polyether. The molecular weight between the cross links is $\sim 33,000$. In general, the degree of polymerization of Carbopol is $\sim 5 \times 10^7$ monomer units resulting in a molecular-weight of 3.5×10^9 g/mole. A typical Carbopol has exceptionally good optical clarity and thickening power even at less than 0.1%(dry weight of carbopol/volume of water), making it very effective and economical. If

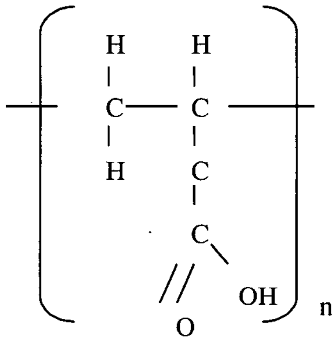

Figure 2.4: Chemical formula of the monomer of the molecule of Carbopol

used at slightly higher concentrations; it produces a transparent smooth gel. It is very versatile in imparting extreme Non-Newtonian properties without excessive elasticity. It is shear thinning in nature and has a yield stress. Two kinds of Carbopol are used in our experiments: Carbopol 940 and Carbopol $EZ2$. In general, the Carbopol $EZ2$ has a lower yield stress than Carbopol 940 for a given concentration.

The yield stress of Carbopol increases with concentration. Carbopol has been described as a micro gel that is a collection of highly cross-linked polymer particles, which individually are gelled but together act effectively as a concentrated dispersion even though the actual concentration is low. The carboxylic groups provided by the acrylic acid backbone of the polymer are responsible for most of its property. Carbopol resins have an average equivalent weight of 76 per carboxylic group. In the form of a dehydrated resin, the molecules of Carbopol are heavily cross linked, which give them strong thickening capacity.

In aqueous system, it is best to achieve thickening by neutralizing the polymer with a base. The neutralization ionizes the polymer and generates negative charge along the backbone of the polymer. Repulsion of like charges then cause the uncoiling of the molecule into an extended structure. This reaction gives instantaneous thickening and emulsion stabilization.

The viscosity of any Carbopol dispersion is sensitive to pH, with a broad maximum in viscosity from around pH $5 - 10$, with a considerable decrease in viscosity above and below this general range. Electrolyte addition also decreases the viscosity, since Carbopol is a polyelectrolyte. On dissolution in water, the pH of the solution is 3.8. This solution is neutralized and brought to a pH of 7 with the help of sodium hydroxide. The addition of sodium hydroxide leads to the development of negative charges on the axes of the polymer. The negative charges repel each other and an entanglement is formed giving rise to a network of chains and gel formation.

Beyond the phase of neutralization that is, pH higher than 9, the repulsion forces between the molecules become stronger and the carboxylic acid group entanglements break leading to the gel disruption.

Finally three zones can be distinguished: for a pH of less than 5, the solution is in a state of pregelification, for a pH between 5 and 8, the solution is in the form of a gel and last of all for a pH higher than 9 the gel breaks down.

2.2.2 Fluid Preparation

Carbopol comes as a fine polymer powder. The powder must be dispersed in an aqueous solution and then an alkaline neutralizer must be added to thicken the solution and to produce a yield stress.

The samples are made from $0.1 - 0.2\%$(dry weight of carbopol/ volume of water), expressed in grams of dry Carbopol powder in $20 - 40$ liters of distilled water. The desired quantity of Carbopol is slowly added to the distilled water for 20 minutes while mixing at a constant rate of $300 - 500$ rpm. The polymer disperses itself very easily. The solution is mixed for $3 - 4$ hours depending on the concentration of the polymer. This is to allow for the complete hydration and mixing of the powder. After the polymer is mixed, the solution is left to rest for 24 hours to allow all air to escape and to allow any foam to break up. It is important to allow all bubbles to disappear before the solution is neutralized. Once the fluid has a yield stress it becomes exceedingly difficult to eliminate bubbles from the fluid.

The fluid is neutralized the next day with the addition of sodium hydroxide (3M) to establish a pH of 7. While mixing at a lower rate (~ 100 rpm), the sodium hydroxide solution is added. We add ~ 125 mL of sodium hydroxide to neutralize the whole sample. In between the solution is left to mix for several minutes. It is important that the rate of mixing is low (~ 100 rpm) so that air is not entrained into the Carbopol. As the sodium hydroxide is added the viscosity of the Carbopol increases and a yield stress develops. Thus, the rate of mixing can be slowly increased with the addition of sodium hydroxide. The addition of sodium hydroxide continues till a pH of $6.5 - 6.8$ is reached and the solution is in the form of a gel with yield stress and then the solution is left to rest for a few hours.

To make the fluid heavier, weighting agent is added to the distilled water before adding Carbopol and is allowed to mix in for about 10 minutes before the addition of Carbopol. The weighting agent used in our experiments is sugar.

Density differences of 5%, 7%, 10% and 13% were achieved. In terms of the fluids used, density difference is defined as:

$$\frac{\rho(displacing)-\rho(displaced)}{\rho(displacing)} \times 100$$

One test run uses two batches of fluids. One fluid is displacing and the other is displaced. For all the tests, the displaced fluid is clear (Carbopol in distilled water) while the displacing fluid is blue; Carbopol colored with food coloring and weighted using sugar. The concentration of sugar was added according to the density difference desired. The pH neutralization followed the same procedure for both the batches of fluids.

2.2.3 Rheological Characterization

Characterization of aqueous Carbopol dispersions was done using Bohlin's controlled stress rheometers (CVO/CVR). Carbopol can be modeled as a Herschel- Bulkley fluid. The rheological parameters of the Carbopol solutions (yield stress, consistency and power law index) are measured using the controlled stress rheometers. These rheometers apply a torque (force) and measure the resultant displacement (movement). Torque and displacement are converted to "rheological" format by means of the measuring system constants.

Selecting Measuring Geometries

Viscometric geometries fall into three basic categories. These are:

1. Cup and Bob.
2. Cone and Plate.
3. Parallel Plate.

Cone and Plate and Parallel plates were used for our fluid characterization and these will be discussed in detail.

1. Cone and Plate:

   Viscometric geometries are referred to by the diameter and the cone angle (Figure 2.5). For instance a CP4/40 is a 40 mm diameter cone having an angle of (4°). The Cone/Plate measuring system consists of a rotating upper cone and a fixed lower plate with a sample contained between them. Since the shear stress is constant (within 0.3%, as per the manufacturer) with radial position for cones with a small cone angle, the viscosity can be calculated directly from the experimental torque/speed rotation. Often cones are truncated. These types of cones are positioned such that the theoretical (missing) tip would touch the lower plate. Since the shear strain and shear rate are calculated using the angular displacement and the gap it follows that the smaller the Cone angle, the greater the error is likely to be in gap setting and hence in the results. By using relatively larger angle (4°) it becomes easier to get reproducibility of gap setting.

   The Cone and Plate geometry should be avoided in case the sample to be tested contains particulate material. Materials with a high concentration of solids are also prone to being expelled from the gap under high shear rates, another reason to avoid the use of the cone.

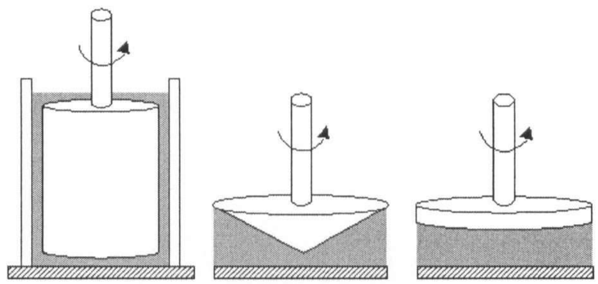

Figure 2.5: (a) Cup and bob (b) Cone and plate (c) Parallel plate.

2. Parallel Plate:

   Parallel Plate geometries are referred to by the diameter of the upper plate. For instance, a PP40 is a 40mm diameter plate. The lower plate is either larger than or the same size as the upper plate. The parallel plates measuring system consists of a rotating upper plate and a fixed lower plate with a sample contained between them (Figure 2.5). The gap between the plates can be adjusted. Unlike the Cone/plate measuring systems, the shear rate is not constant with radial position, but varies from zero at the center to a maximum at the edge. The induced shear rate is inversely proportional to the gap size. Parallel plate has the advantage of being able to take preformed sample discs which can be especially useful when working with polymers. It is not sensitive to gap setting, since it is used with a separation between the plates measured in mm. Because of this it is ideally suited for testing samples through temperature gradients.

   The main disadvantage of parallel plates comes from the fact that the shear rate produced varies across the sample.

   Hence, it is best to test thick materials with a Cone and Plate unless they contain particulate matter, in which case use of parallel plate is recommended.

Testing Procedure - Characterization

The tests are done at a constant temperature of 22 °C , which is approximately the temperature of the laboratory in which the experiments are conducted. The temperature changes by $1-2$ °C during the tests. The temperature change does not have any effect on the tests. The compressed air line is switched on and the pressure is set at 3 bar (300 KPa). The computer is switched on. The measuring geometry is inserted into the rheometers. The CVOR is held at zero position (i.e. where the cone just touches the lower plate) automatically by pressing the key marked ZERO on the CVOR front panel. When the OK light comes on the panel, the required gap is set by pressing the GAP key on the panel. In case of a 4/40 cone, the required gap is 0.15 mm on the CVOR. It is important to have the correct gap setting for each measuring system since the correct gap between the upper and lower measuring systems are essential for accurate measurements. An incorrect gap will lead to errors in the results, especially when small gaps or small cone angles are involved.

A correct amount of sample is loaded. Usually, we put $2-3$ drops of the sample between the upper and the lower measuring systems. Over filling or under filling results in the errors in the data. Test protocol is selected and the sample is subjected to the required tests. Since in general, it is difficult to accurately measure the yield stress of a sample, we apply the principal of Hooke's law to find the accurate value of yield stress (Figure 2.6). This law states that the stress is directly proportional to the strain, up to a limit called the proportionality limit. Physically, this limit can be explained as the region up to which the fluid responds elastically. This limit is called the yield stress of the fluid. When the yield stress is exceeded, the properties of the fluid are changed and it exhibits plastic deformation. The yield stress is directly measured by successive creep/recovery tests. A constant stress is applied to the sample and the strain response after 400 s is measured. We normally increase the applied stress between successive tests by $1Pa$. When the strain response is plotted versus the applied stress there is a stress value above which the strain response begins to increase significantly as a function of the applied stress. The stress value at which this occurs is defined to be the yield stress. The measurement of the yield stress can be made to an accuracy of about $\pm 0.2Pa$.

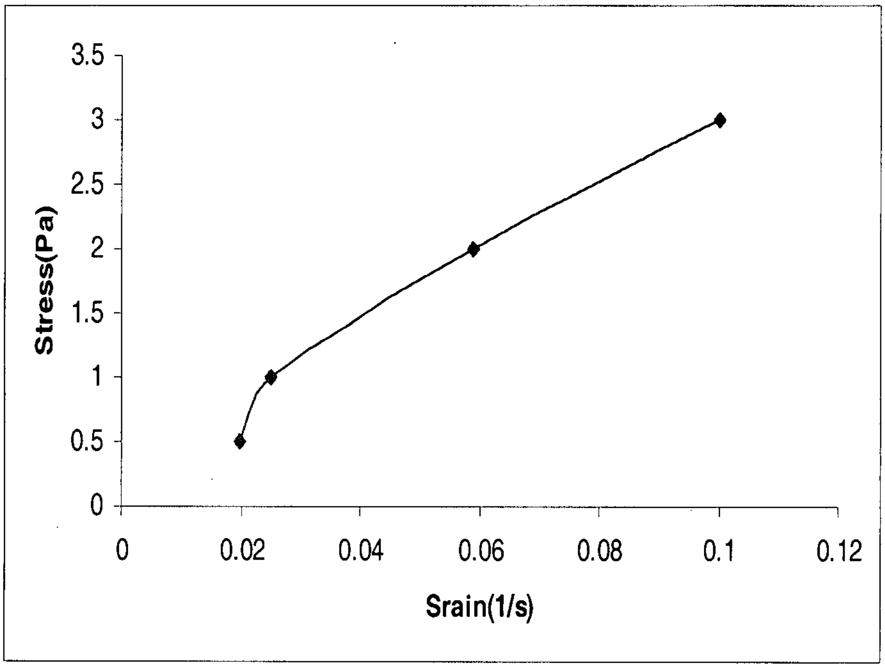

Figure 2.6: Yield stress ($1Pa$) of a Carbopol 940 - 0.1% (dry weight of carbopol/volume of water) sample.

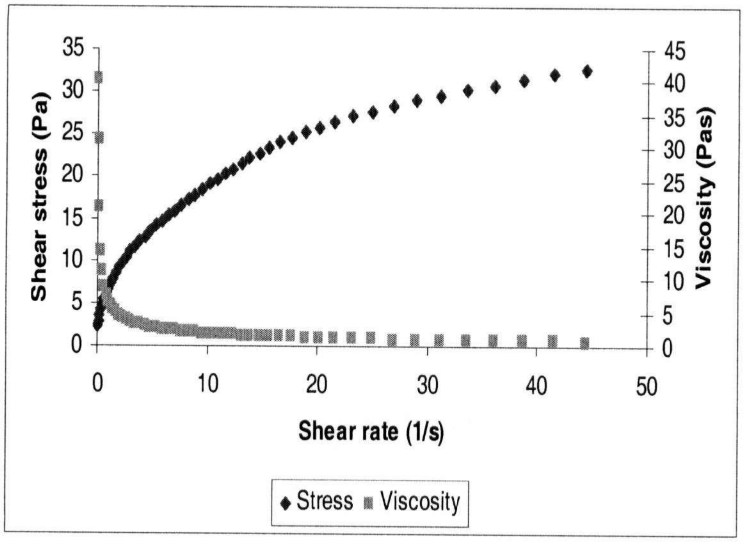

Figure 2.7: Typical flow curve for the viscometry test from the controlled stress rheometer 940 – 0.1%(dry weight of carbopol/volume of water)

The consistency and power law index are determined from a controlled stress viscometry test, where the rate of strain is measured at various stresses. A typical flow curve from the controlled stress rheometer is shown in Figure 2.7.

Having already found the yield stress, the consistency and the power law index are fitted to the data in a least square fit and hence calculated.

2.2.4 Experimental Procedure - Displacement Process

Briefly, the experiments involve displacement of one fluid by another in the annular space between the two tubes.

Tank A (Figure 2.8) is filled up with the fluid 1 (displaced) and tank B with the fluid 2 (displacing). The valve $V3$ leading to the bubble column is closing and the valve $V4$ leading to the small pump is set open. The one way valve $V6$ leading to the manifold is also closed.

For purging the lines with the white fluid 1, another valve $V5$ prior to the one way valve is set open and the small pump is started. The fluid runs through the 6 lines and the lines are filled up with the white fluid. Valve $V5$ is then closed and the one way valve $V6$ is set open again. It is important to purge all the lines with the fluids to avoid suction of air during the displacement process, which can alter the test results. The fluid 2 from tank B is passed through the flow meter by opening the valve $V1$ and its velocity is calibrated using the flow meter. Once the fluid is set at a particular velocity, the fluid passes through the big pump to the distribution manifold. There is a set of 6 valves at each end. Each of these valves is used to purge the 6 inlet lines with the fluid first by opening them one by one. Once the lines are filled up with the displacing fluid, the valves are open and the displaced fluid 1 is pumped into the annulus with the help of the small pump. Once the fluid fills up the entire annular space, the displacing fluid 2 is pumped into the annulus with the help of big pump. Displacement begins as soon as the interface moves forward in the annulus. Within the time scale of the displacement process the shape of the interface changes continually. The nature of the interface depends on the position in the gap and material properties of the two fluids and dynamics of the flow. The velocity of the displacing fluid 2 is determined by the flow meter The test is stopped when the blue fluid reaches the end of the annulus. Unsteady displacement of two Carbopol solutions is shown (Figure 2.10). To clean the annulus, the main inlet lines leading to the annulus are switched so that the fluid now enters from the top of the annulus. The annulus is cleaned up by running 2 M sodium hydroxide through it from the top. The solution is prepared using distilled water mixed with sodium hydroxide pellets. It is allowed to rest for 10 mins since the preparation process is exothermic and the solution needs to be cooled down. The annulus is purged with air, water and sodium hydroxide until the whole tube is clean. Then it is rinsed with water by running water through the tube for 5 mins so that there are no traces of sodium hydroxide left in the tube. The status of valves under the test conditions is shown (Figure 2.9).

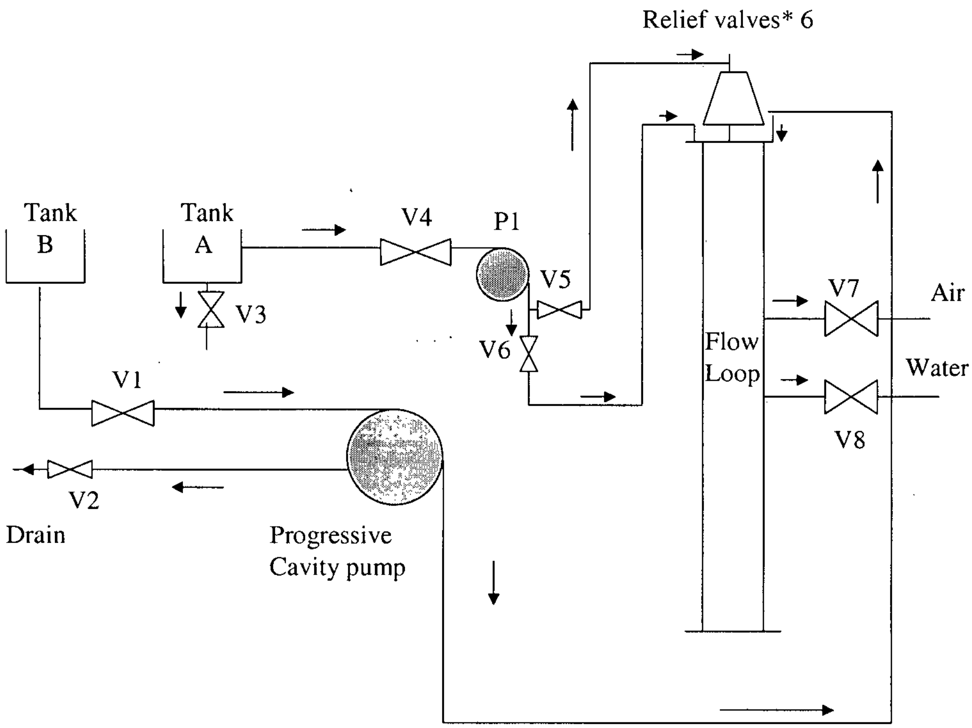

Figure 2.8: Schematic of annular flow loop

2.2.5 Experimental Plan

The experimental plan is designed to investigate the effects of primary factors, i.e. annular geometry, inclination β , eccentricity e , density difference, flow rate, controlled concentration and pH of the two carbopol fluids. The dimensions of the annulus are fixed. It is difficult to observe and control interactive effects of the parameters. Also, any factorial design is infeasible i.e. we cannot map out parameter space completely. The experiments were spaced out in such a manner that thirty-six experiments were performed with a measurement of all the parameters. Individual parameter space is discussed in the section below:

Fluid Combinations used

It is required to have a higher yield stress ($7 - 9$ Pa) fluid displace a lower yield stress ($1 - 3$ Pa) fluid for the displacement to be stable. Concentration of 0.1% is chosen to have a lower yield stress fluid. Concentration of 0.2% is chosen to have a higher yield stress fluid. It is also

Mode	**Open**	**Closed**
Calibration	1(a)	2, 3, 4
To flow loop (from Tank B)	1(b)	2, 3, 4
To flow loop (from Tank A)	4(b)	4, 3, 1
To switch lines	4(a)	2, 3,1
To drain	3	2, 1,4

Valve 2	Valve 1(a) Valve 1(b)
Valve 4(a) Valve 4(b)	Valve 3

Figure 2.9: Status of valves and valve system under test conditions.

required to analyze the effects of two different fluids, Carbopol 940 and Carbopol $EZ2$ on the displacement process when both the fluids are used for the experimental run. Following combinations are used for our experiments:

1. Carbopol 940 (0.1 %(w/v), $pH \sim 5.8$) with Carbopol 940 (0.2 %(w/v), $pH \sim 6.4$)
2. Carbopol $EZ2$ (0.1 %(w/v), $pH \sim 5.3$) with Carbopol $EZ2$ (0.2 %(w/v), $pH \sim 6.5$)
3. Carbopol $EZ2$ (0.2 %(w/v), $pH \sim 6.5$) with Carbopol 940 (0.2 %(w/v), $pH \sim 6.8$)

With 0.2% always being the more viscous (displacing) fluid and 0.1% being the less viscous (displaced) fluid. A more viscous fluid is always used to displace a less viscous fluid. The concentrations used represent known dry weight of carbopol in known volume of water. Flow curves for all three fluid combinations are shown (Figures 2.11, 2.12 and 2.13).

The viscosity of a fluid indicates its resistance to flow. A more viscous fluid has higher resistance to flow while a less viscous fluid has lower resistance to flow.

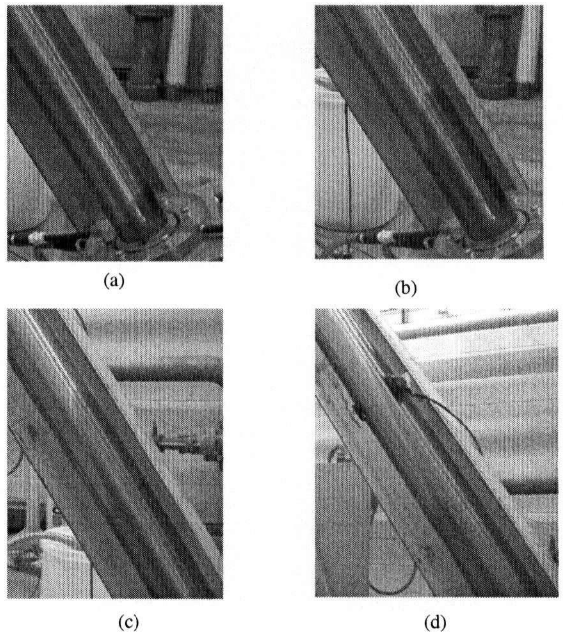

Figure 2.10: Unsteady displacement of two aqueous Carbopol solutions

Flow Rate

The flow meter is calibrated to the desired flow-rate (8l/min-20l/min) for each experimental run. Mean velocity of the fluids is also calculated. The displacement process is recorded with ease at the given flow rates. The flow meter is magnetic and it responds differently to the magnetic content of the fluid. Therefore for each experimental run, flow rate is calibrated and not varied during the experiment. The flow rate is measured to an accuracy of $\pm 0.5\%$.

Inclination

We focus our attention on displacements in near - vertical oil wells. The test is run at four different angles: 15, 20, 30 and 45 degrees. Due to safety considerations, $0 - 15$ degrees inclination is not considered as the annulus when raised at 0 degrees hits the roof. By changing inclination we wish to investigate whether displacement efficiency declines with deviation from the vertical.

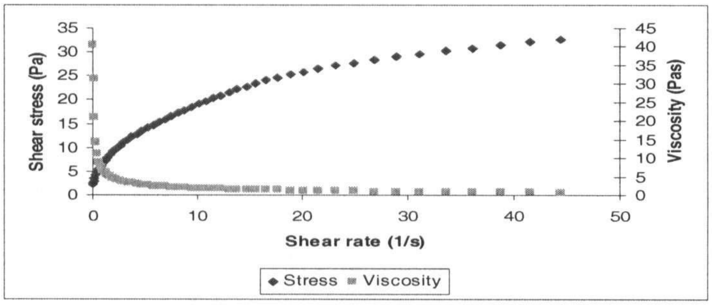

(a)

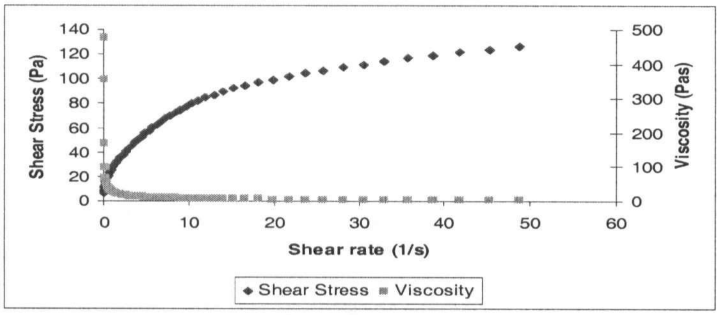

(b)

Figure 2.11: Flow curves for fluid combinations used (a)940 – 0.1% (w/v)(b) 940 – 0.2% (w/v)

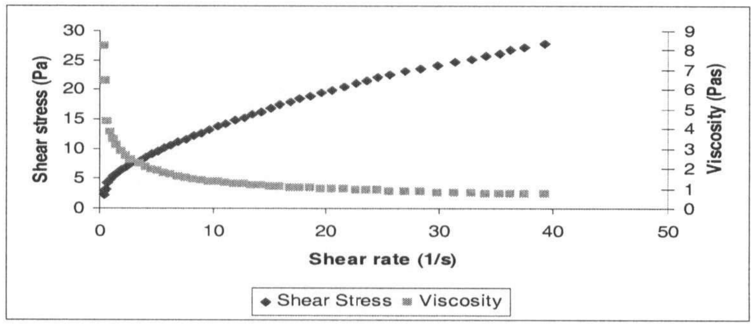

(a)

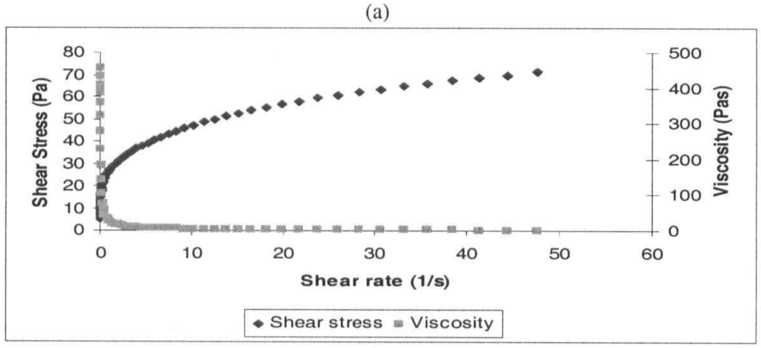

(b)

Figure 2.12: Flow curves for fluid combinations used (a) $EZ2 - 0.1\%$ (w/v)(b) $EZ2 - 0.2\%$ (w/v)

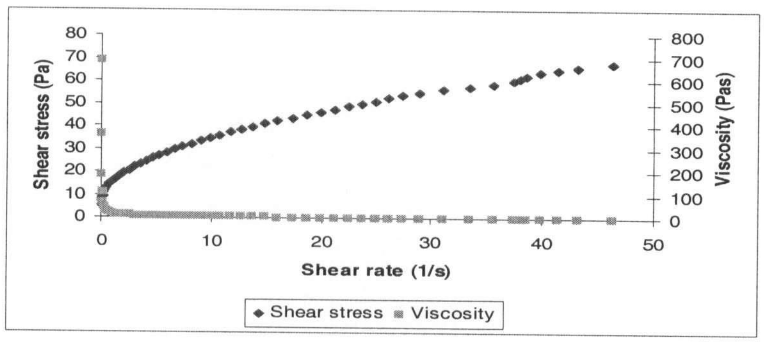

(a)

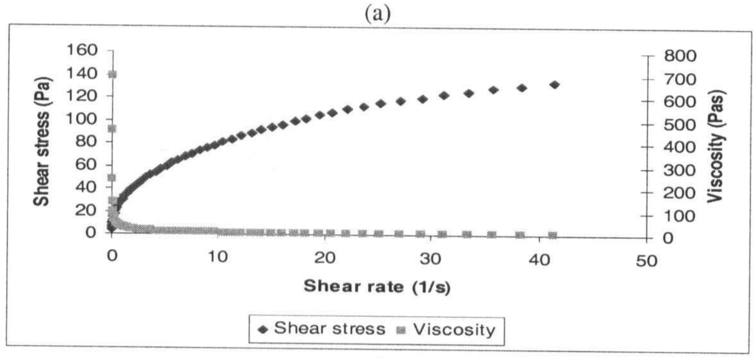

Figure 2.13: Flow curves for fluid combinations used (a) $EZ2-0.2\%$ (w/v)(b) $940-0.2\%$ (w/v)

Density

Three ranges are chosen for considering the density effects: Isodensity, 5% density change and 10% density change between the displaced and displacing fluids with the displacing fluid being the heavier and denser. We wish to investigate the effect of a positive density contrast between the two fluids on the displacement process. Also, industrial practice is to have a higher density difference (10%) between the two fluids. Attention is focussed on implementing industrial rules. Isodensity and 5% density difference are chosen to consider the effects of no or lower density. Density is measured to an accuracy of $\pm 29 kg/m^3$.

1. Isodensity series:

   $\frac{\rho_2-\rho_1}{\rho_2} = 0\%$

   All the fluid samples are prepared in distilled water and have a density of $\sim 1000 kg/m^3$. Three experiments each with $e = 0$, $e = 0.2$, $e = 0.3$ and $e = 0.5$ are run. All 12 experiments for the isodensity series are observed with different concentrations of each fluid. Flow rate and inclination are measured for each run and the data is recorded.

2. Density Change $\sim 5\%$:

   $\frac{\rho_2-\rho_1}{\rho_2} = 5\%$

   Fluid 2 (displacing) is prepared in such a manner that it is more viscous and heavier (by addition of sugar) than fluid 1 (displaced). Fluid 2 has a density of $\sim 1185 kg/m^3$ and fluid 1 has a density of $\sim 1000 kg/m^3$. The data is observed at various eccentricities as above and flow-rates is recorded. Twelve such experiments are run and observations made.

3. Density Change $\sim 10\%$:

   $\frac{\rho_2-\rho_1}{\rho_2} = 10\%$

   Fluid 2 is made 10% heavier and viscous than fluid 1. Fluid 2 has a density of $\sim$ $1201 kg/m^3$ and fluid 1 has a density of $\sim 1000 kg/m^3$. Again, twelve such experiments are run at various eccentricities as above and flow rates are recorded.

Eccentricity

To observe the effect of eccentricity, tests are run at three different eccentricities starting with: $e = 0$, $e = 0.2$, $e = 0.3$ and $e = 0.5$. Attention is focussed on concentric ($e = 0$)and eccentric annulus. Also, it is desired to consider the effect of increasing eccentricity in the annulus. Eccentricity is measured to an accuracy of gap $\pm 0.005mm$.

The experimental matrix for all thirty-six experiments consists of flow rates in the range $11 - 20$ l/min, eccentricities (0, 0.2, 0.3 and 0.5), inclinations (15, 20, 30 and 45 degrees), density differences of (0 %, 5 %, 10 %) and fluid concentrations (0.1 %, 0.2 %). The matrix is designed to allow detection of interactions between various effects.

Analysis of the experimental accuracy is discussed in Chapter 4 of this thesis.

Chapter 3
Model

3.1 Lubrication Model

The main objectives of modeling the annular flow is to simulate the behavior of the interface between fluids so as to determine the type of displacement that occurs given the specific rheologies, densities and geometry of the annulus. It is considered that three main situations can occur:

1. A stable steady displacement with both fluids fully moving and the interface stationary moving in a frame of reference with the average speed of the flow;
2. An unsteady displacement with both fluids moving and the interface advancing ahead of the mean speed of the flow on the wide side of the annulus, i.e. the interface elongates;
3. Static channel with either the displaced fluid or both fluids stationary on the narrow side of the annulus and the interface between them elongating.

Hence we employ techniques used in modeling of lubrication and thin film flows to derive a criteria for determination of the type of annular-displacement occurring.

3.1.1 Determining the displacement type

The displacements are classified according to the behavior of the flux function $q(\Phi_i)$ - which is the stream function at the interface. Our classification will be based on the wide and narrow side interface velocities, which we must determine from q. The interface speed depends primarily on the shape of $q(\Phi_i)$. Note that Φ_i is actually a volumetric position of the interface, i.e. the volume fraction of fluid 2 at depth ζ. From this, in the absence of shocks, [13], we obtain the speed of propagation of the interface in the ζ- direction:

$$W_i = \frac{\mathrm{d}\zeta}{\mathrm{d}\Phi_i}\frac{\mathrm{d}q}{\mathrm{d}\zeta} = \frac{\mathrm{d}q}{\mathrm{d}\Phi_i} = q'(\Phi_i), \tag{3.1}$$

q is computed for given fluid densities, rheologies, angle of inclination and eccentricity. We denote the wide and narrow side interface velocities by $W_{i,w}$ and $W_{i,n}$, respectively. In the model, the 0 corresponds to the wide side of the annulus and 1 corresponds to the narrow side of the annulus. We classify the displacement according to the values of $W_{i,w}$ and $W_{i,n}$ which must be determined from $q'(\Phi_i)$ as follows:

1. Static Channel: If $q'(1) = 0$, then a static mud channel occurs on the narrow side of the annulus and the fluid 1 is unyielded here. The displacement is thus not steady and the interface continues to elongate.

2. Stable: If $q'(0) < 1$ and $q'(1) > 1$, the fluid is yielded everywhere. This says that an elongating wide-side finger cannot exist. This displacement is classified as stable.

3. Unsteady: If $q'(0) > 1$ and $q'(1) < 1$, the interface moves faster on the wide side than the narrow side and the finger- like interface continues to elongate i. e. The fluid 1 slumps on the narrow side of the annulus and fluid 2 advances up on the wide side.

4. Indeterminate: If $q'(0) < 1$ and $q'(1) < 1$

   The q plots as predicted by the model for both an eccentric and concentric annulus are shown in Figure 3.1 , 3.2 and 3.3

More details regarding the classification can be found in [13] .

3.1.2 Model derivation

The overall idea is to assume a highly elongated interface that is more advanced on the wide side than on the narrow side. This is the situation we wish to identify, for both unsteady displacements and for static mud channel formation. Assuming that streamlines are

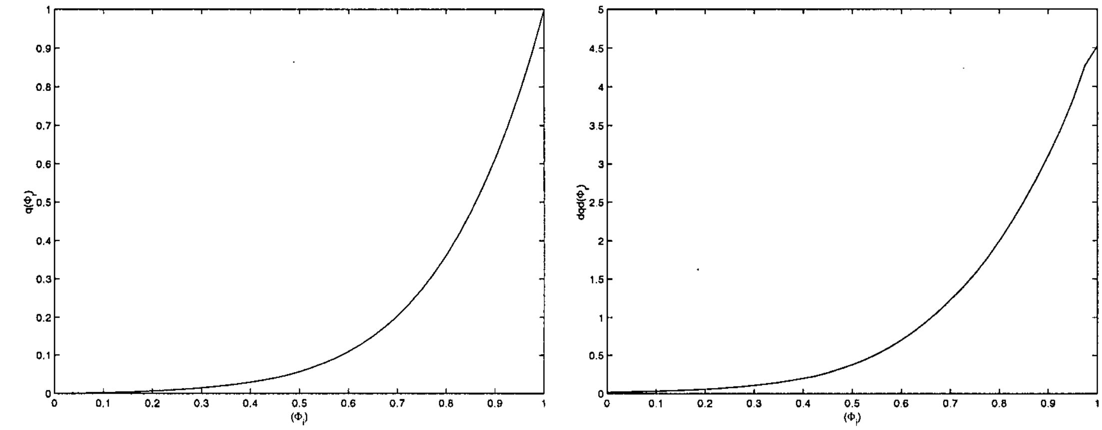

Figure 3.1: Stable displacement in an eccentric annulus

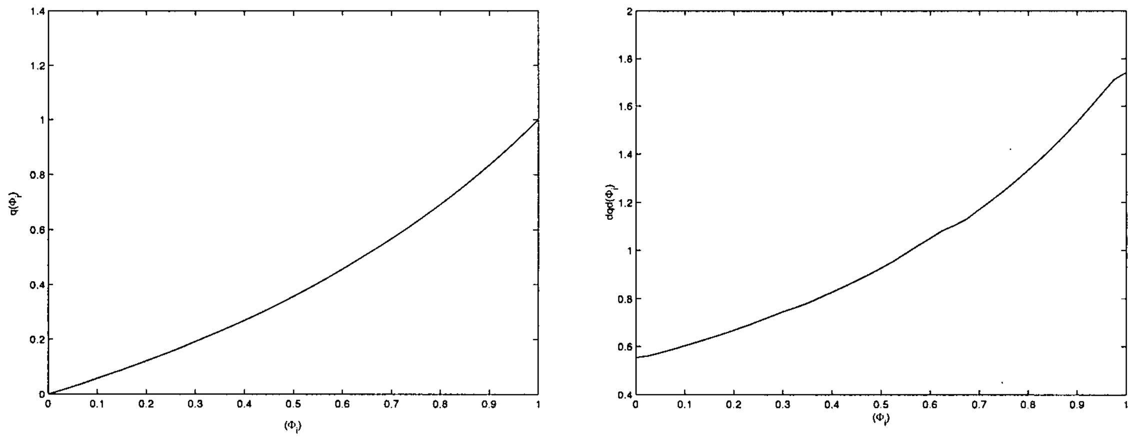

Figure 3.2: Stable displacement in a concentric annulus

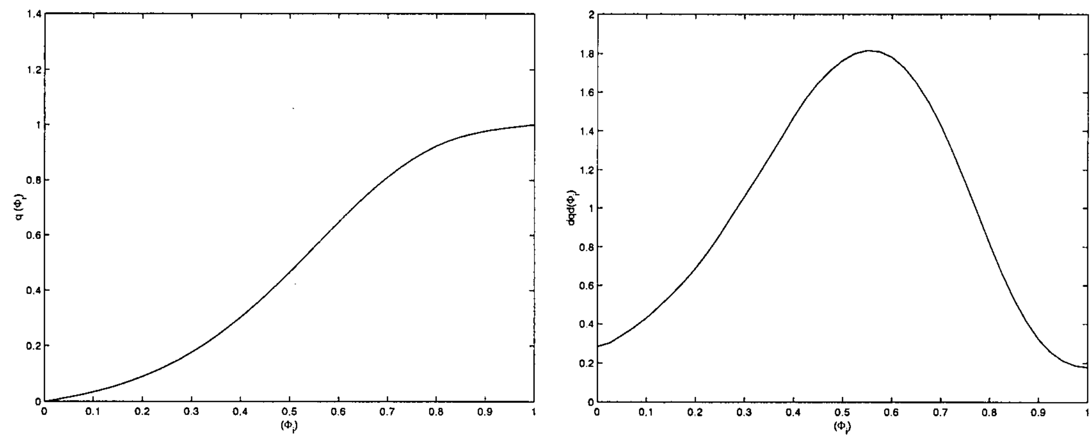

Figure 3.3: Indeterminate displacement.

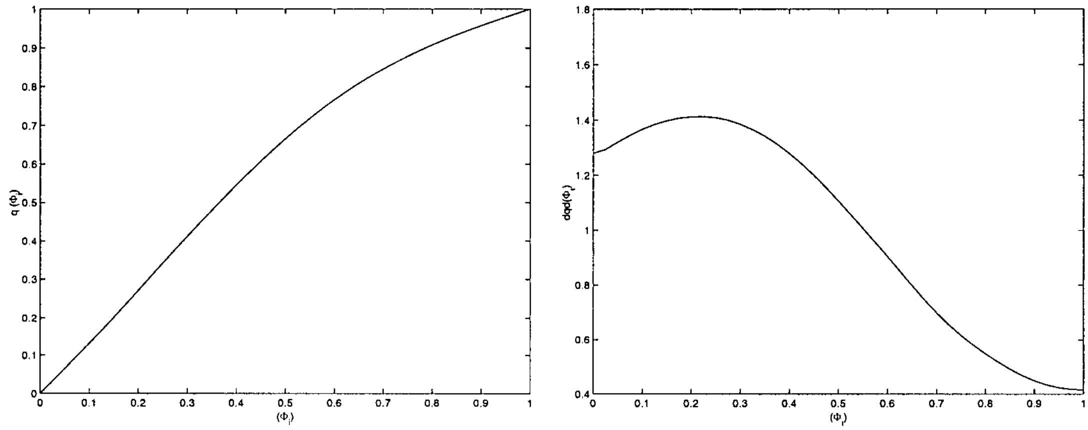

Figure 3.4: Unsteady displacement in an eccentric annulus.

pseudo-parallel with the annular axis, a lubrication or thin layer model for the displacement is derived and then the model is analyzed to predict the interface speed, on both wide and narrow sides of the annulus; see [13] for details. The computed interface speed helps us classify the displacement , 1-3, as above.

In the absence of shocks, the interface speed is simply the characteristic speed:

$$W_i = \frac{\mathrm{d}q}{\mathrm{d}\Phi_i} = q'(\Phi_i). \tag{3.2}$$

This is obtained from the hyperbolic equation for the interface given by:

$$\frac{\partial \Phi_i}{\partial t} + \frac{\partial}{\partial \zeta} q(\Phi_i) = 0 \tag{3.3}$$

which gives the speed of propagation of the interface.

To find $q(\Phi_i)$, we start with the annular half-gap width defined by

$$H = 1 + e \cos \pi \phi \tag{3.4}$$

where $e \in [0, 1]$ is the annulus eccentricity; $e = 0$ corresponds to a concentric annulus, $e = 1$ implies contact between casing and outer wall, on the narrow side of the annulus.

The volumetric interface position is defined by:

$$\Phi_i = \int_0^{\phi_i} H(\phi)\ \mathrm{d}\phi = \phi_i + \frac{e}{\pi} \cdot \sin \pi \phi_i, \tag{3.5}$$

i.e. Φ_i represents the volume fraction of fluid 2 at a certain depth ζ. The relationship between Φ_i and ϕ_i is one to one, so we may write $\phi_i = \phi_i(\Phi_i)$

We need to find the modified pressure gradient in fluid 2, which we find using the boundary condition at $\phi = 1$, i.e.

$$\int_0^{\phi_i} \frac{\partial \Psi}{\partial \phi}(G_1)\ \mathrm{d}\phi + \int_{\phi_i}^1 \frac{\partial \Psi}{\partial \phi}(G_2)\ \mathrm{d}\phi = 1 \tag{3.6}$$

which represents simply finding the pressure gradient to satisfy an imposed flow rate through the annulus. It follows that the above equation is simply a nonlinear equation for G, which is the modified pressure gradient in the displacing fluid 2. Furthermore, it is straightforward to show that the flow rate Q(G):

$$Q(G) = \int_0^{\phi_i} \frac{\partial \Psi}{\partial \phi}(G_1)\ \mathrm{d}\phi + \int_{\phi_i}^1 \frac{\partial \Psi}{\partial \phi}(G_2)\ \mathrm{d}\phi \tag{3.7}$$

increases strictly monotonically with G. Continuity of pressure at the interface means that the same pressure gradient acts in the axial direction in each fluid layer, but is modified in each fluid by the different densities.

3.2 Computational methods

To derive the lubrication model, we non-dimensionalise and re-scale the equations above. We take the relevant dimensional scales from our experimental data

3.2.1 Non-dimensionalisation

Scalings

To scale the velocities we define a typical cross-section of annulus $\hat{A}^* = \pi[\hat{r}_o^2 - \hat{r}_i^2]$ and a scale for the flow rate $\hat{Q}^* = \hat{Q}_{pump} \times \frac{0.001}{60}$. The annulus gap size is scaled as $\hat{d}^* = 0.5 \times [\hat{r}_o - \hat{r}_i]$. The velocity scale is defined by $\hat{w}^* = \hat{Q}^*/\hat{A}^*$.

To scale the fluid properties, we define a scale for the rate of strain by $\hat{\dot{\gamma}}^*$:

$$\hat{\dot{\gamma}}^* = 3 \times \frac{\hat{w}^*}{\hat{d}^*}, \tag{3.8}$$

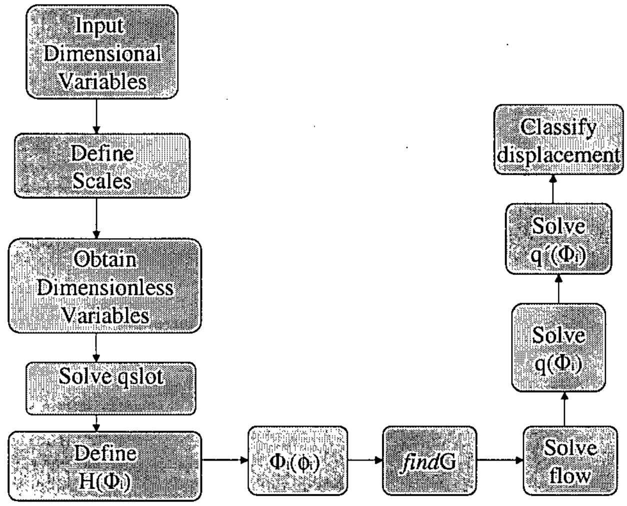

Figure 3.5: Sequential flowchart of sub-routines

Our scale for the shear stress is given by $\hat{\tau}^* = 10$. This is the maximum value of stress used for our experiments.

and we use this to define a scale for viscosity, as follows: $\hat{\mu}^* = \dfrac{\hat{\tau}^*}{\hat{\dot{\gamma}}^*}$.

The fluid densities are scaled with $\hat{\rho}^* = 1000$

Stokes number is defined by $St^* = \frac{\hat{\tau}^*}{\hat{\rho}^* \hat{g}^* \hat{d}^*}$

The buoyancy parameter b is given by: $b = \frac{\rho_2 - \rho_1}{St^*} \cos\beta$

3.2.2 Flowchart

A sequential flowchart of our code is shown in figure 3.4. Our final sub-routine is called *main* which takes input from all the subroutines shown in the flowchart. Methodology of each sub-routine is discussed in the next section.

3.2.3 Sub-routines

The sub-routines for the model were written in MATLAB. The computational methods used are explained below:

We write linear interpolation method to solve for $\dot{\gamma} = f(\tau)$ where τ is simply defined as

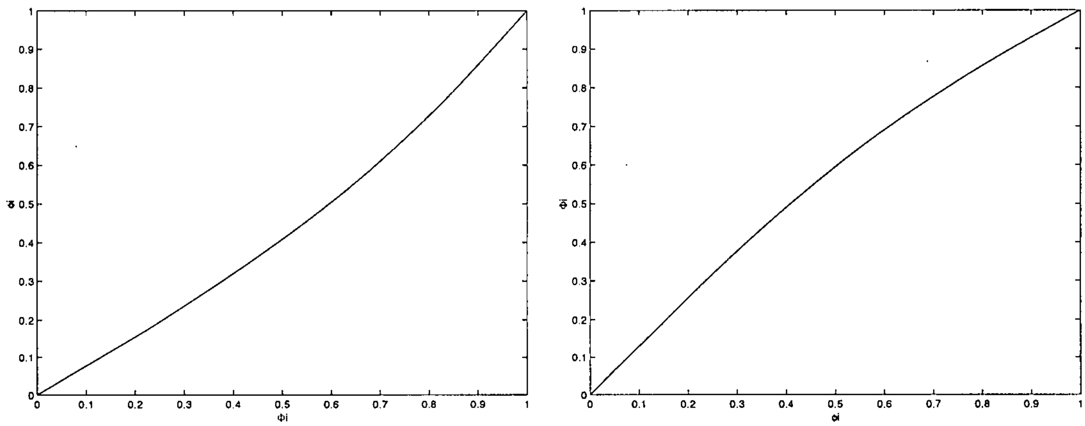

Figure 3.6: Plots of $\phi_i = \phi_i(\Phi_i)$ and $\Phi_i = \Phi_i(\phi_i)$

$\tau = Gy$. We write a sub-routine called *qslot* which is computed as follows:

$$qslot = \int_0^H y\dot{\gamma}(Gy)dy \tag{3.9}$$

Using integration by parts, we see that this is the integral of the velocity across a slot of half - width H. This is calculated for both the fluids, i.e. fluid 1 and fluid 2.

Equation 3.4 and 3.5 are used to find the volumetric interface position. Newton's method is used to compute $\phi_i = \phi_i(\Phi_i)$. Both functions are computed as shown in the figure 3.5

To solve equation 3.6, we need to find the modified pressure gradient G. Since, we need to use a root finding technique to solve for G, this sub-routine uses an incremental search method to bracket the root and the bisection method for finding an appropriate value of G. To solve equation 3.7, Simpson's rule is used twice to solve the integrals used in equation 3.7. It integrates *qslot* from $0 - \phi$ and from $\phi - 1$ for fluids 2 and 1 respectively. Once the value of G is found, the first integral in the equation 3.7 as denoted *qphii*.

We then differentiate *qphii* numerically to get the interface velocity, called *dqdphii*.

The final sub-routine called *main* takes the input from all these sub-routines in the order shown above in the flowchart and returns plots of q and q'. We then classify displacement as stable or unsteady as explained in section 3.1.1.

Chapter 4
Results

4.1 Experimental results

This section presents the experimental results. We then make comparisons against the equivalent theoretical and numerical predictions.

In eccentric annuli, the 0° position corresponds to the wide side of the annulus, with narrowest part at 180°. We investigate the effects of various parameters on laminar displacement of two non-Newtonian fluids in an annulus with variable eccentricity and inclination. This section analyzes the effects of factors explained in section 2.2.5, i.e. eccentricity, density difference, inclination, flow rate and concentration on displacement of two fluids with competing rheologies.

Thirty six experiments were conducted using three different combinations of Carbopol $EZ2$ and Carbopol 940.

Effect of density difference Density difference has a positive effect on displacement in a concentric annulus. As we increase the density difference to 10 %, some of the displacements observed are stable with a flat interface between the two fluids. For an isodensity displacement, flow bypass is observed; see section 4.1.1.

In an eccentric annulus, density contrast can make significant improvement in displacement in the narrow side. Experiments classified as stable and unsteady for a fixed density difference for various inclinations and eccentricities are shown in Figure 4.1. As can be seen from the

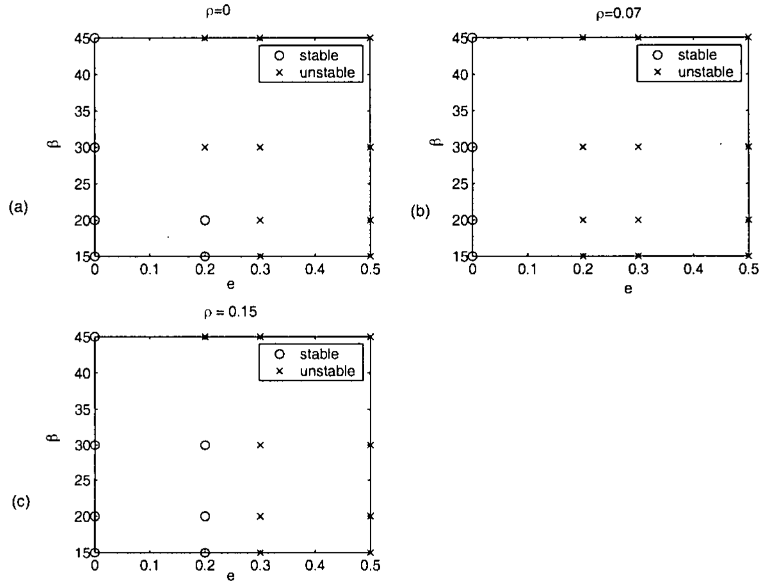

Figure 4.1: Stable and unsteady regimes for a fixed density difference at various inclinations and eccentricities ((a) $\rho = 0$; stable - $e = 0$, $e = 0.2$ for $\beta = 15, 20$ degrees; unsteady -$e = 0.3, 0.5$. (b) $\rho = 0.07$; stable - $e = 0$; unsteady - $e = 0.2, 0.3, 0.5$ and (c) $\rho = 0.15$; stable - $e = 0$, $e = 0.2$ for $\beta = 15, 20, 30$ degrees ; unsteady - $e = 0.3, 0.5$.)

Figure 4.1, as we increase the density contrast to 15%, the stable displacement regime increases from $e = 0$ to $e = 0.2$. For $e = 0.3$ and $e = 0.5$, from our experimental findings, it is generally observed that a 10-15% density contrast aids in the movement of the fluid on the narrow side of the annulus.

In an eccentric annulus, where the displacing fluid has a tendency to channel through the wide side, a positive density difference between the two fluids produces a hydrostatic pressure imbalance between the wide and narrow sides. This imbalance imposes a secondary azimuthal current on the main axial flow whose direction is from the narrow to the wide side of the annulus. Thus, azimuthal flow can improve the mud removal in the narrow side.

Effect of eccentricity A decrease in the casing centralization can be due to a variety of reasons including inclination of the hole, uneven cuttings or mud cake buildup, washout etc. In such instances displacement is accelerated in the wide side, leaving slow moving mud behind in the narrow side of the annulus.

It is observed that $e = 0.5$ reduces the overall efficiency significantly. This is maximum value of eccentricity used for our experiments. Channeling occurs in some cases with hardly any

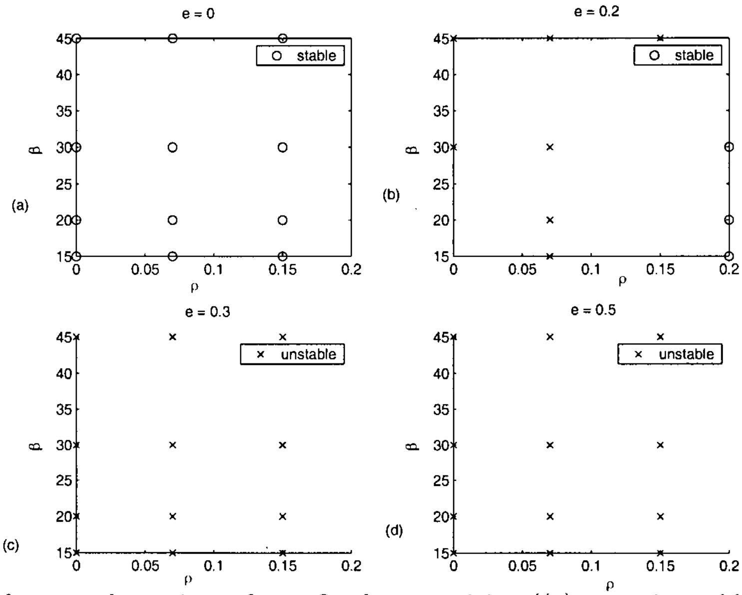

Figure 4.2: Stable and unsteady regimes for a fixed eccentricity ((a) $e = 0$; stable at all inclinations and all density contrasts. (b) $e = 0.2$; stable - density contrast of 20% at $\beta = 15, 20, 30$; unsteady - 0 and 7% density contrast. (c) $e = 0.3$; unsteady at all inclinations and density contrasts (d) $e = 0.5$; unsteady at all inclinations and density contrasts.)

movement on the narrow side of the annulus. The fluid extends on the wide side, forming a finger which continues to grow. The negative effect of eccentricity, for $e = 0.5$, becomes less significant as density contrast is increased to 15%. Further reductions in eccentricity, however, appear to increase the rate of displacement. The overall efficiency exhibits a minimum around $e = 0.5$. For $e = 0.3$, finger formation and break-up is observed. For e=0.2, stable displacement is observed for a few cases but for most cases unsteady displacement is observed.

Stability of the displacement is affected as we increase the eccentricity with the interface being stable.

Experiments classified as stable and unsteady for a fixed eccentricity are shown (Figure 4.2).

Effect of Inclination The dynamics of mud displacement is affected by the angle of deviation of the annulus from the vertical. In the experiments conducted, displacement was carried out at inclinations of $15, 20, 30, 45$ degrees from the vertical.

In an eccentric annulus, with an $e = 0.5$, there is a negative effect of inclination. Displacement deteriorates as inclination increases. The effect is not that significant until ϕ is well above

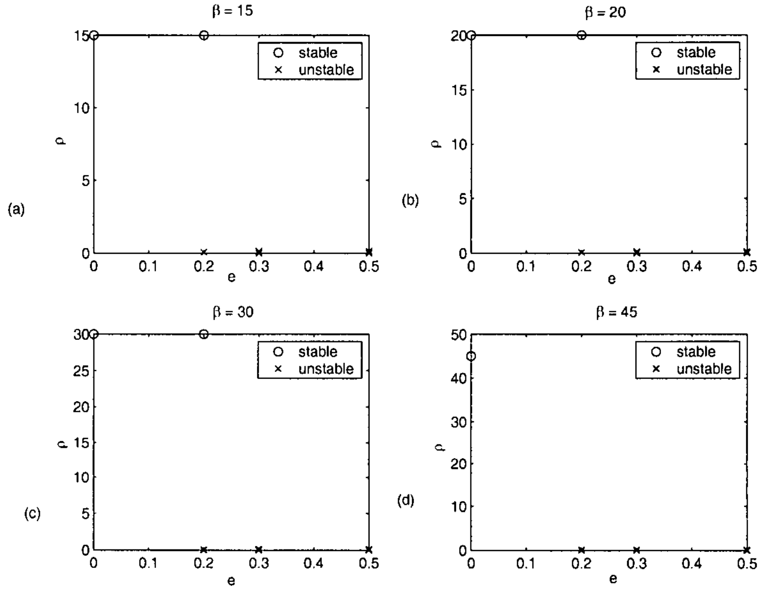

Figure 4.3: Stable and unsteady regimes for a fixed inclination(mostly unsteady: 20, 30, 45 degrees at e = 0.2, e = 0.3 and e = 0.5.)

30°. This effect is less pronounced as the eccentricity is reduced and the density contrast is increased.

Experiments classified as stable and unsteady for a fixed inclination are shown (Figure 4.3).

Effect of rheology Rheology of the two fluids is related to their concentration. To maintain a lower yield stress of $\sim 1-2Pa$ and consistency of $\sim 3-13Pas^n$, the concentration of a carbopol sample was taken as 0.1%. Higher yield stress of $\sim 5-9Pa$ and consistency of $\sim 30-140Pas^n$ can be obtained by maintaining the concentration of a carbopol sample of 0.2%.

In a negative rheology difference, the displacing fluid has lower yield stress than the displaced fluid. It also has a lower flow curve range than the displaced fluid for our experiments. This reduces the overall efficiency in laminar displacement. This can result in severe channeling. A positive rheology difference tends to flatten the interface between the two fluids and improve the displacement process.

From our experimental findings the trend observed is shown in Figures 4.1, 4.2 and 4.3.

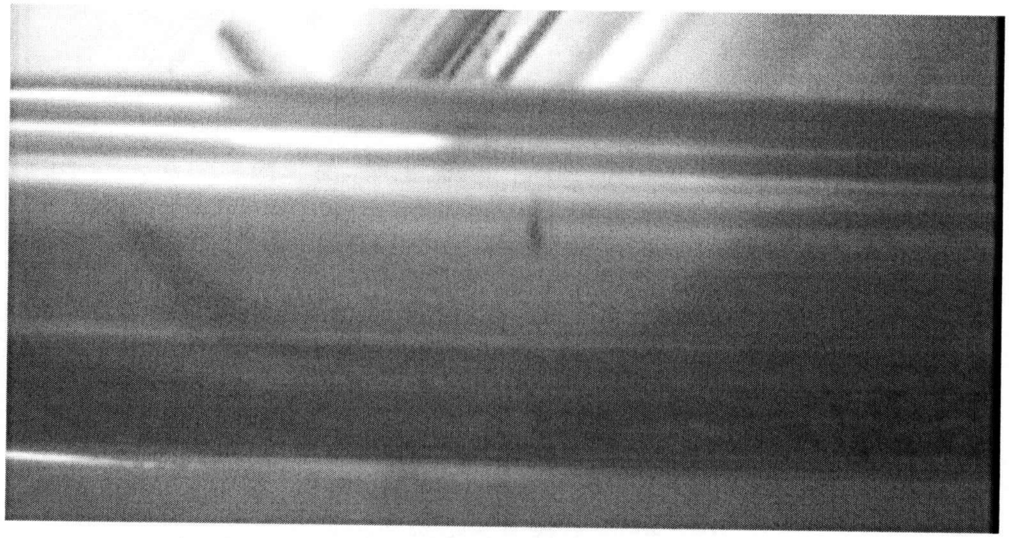

Figure 4.4: Onset of Flow bypass- fluid 1 takes the shape of a droplet and is left behind on the wide side of the annulus eventually.

Effect of flow rate Higher flow rates of $16.6l/min$ improve the displacement process. The displacement is stable at higher flow rates while the displacement is unsteady at lower flow rates $(8 - 12l/min)$.

4.1.1 Flow bypass

Our flow visualization experiments indicate that under certain conditions flow bypass occurs.

Initially the annulus is filled up with the displaced Fluid 1, the displacing Fluid 2 enters the annulus. Initially it displaces the Fluid 1 thus making the interface move forward but it bypasses the Fluid 1. Fluid 1 in the shape of a large droplet is left behind on the wide side of the annulus, while the interface continues to move forward. The droplet shaped position of Fluid 1 that is left behind keeps on growing without breaking up(Figure 4.4). Schematic of the flow bypass is shown (Figure 4.5). In certain experimental runs, this phenomena occurs

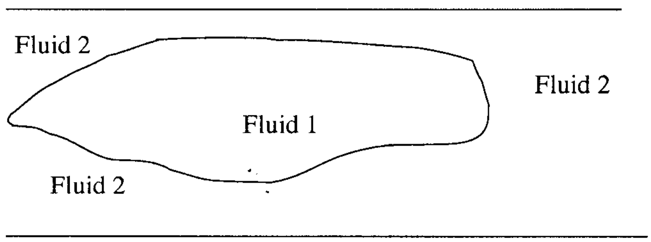

Figure 4.5: Schematic of flow bypass

twice along the length of the annulus.

As we increase the eccentricity, flow by pass is overcome and unsteady interface is observed. This phenomena can be found for a few experimental runs for $e = 0.2$ and for a very few cases for $e = 0.3$. It is not found for $e = 0.5$.

To our knowledge, there are no reports of such instabilities in the literature. Our observations show that for a concentric annulus, with positive rheology difference, with or without density difference, at all angles there is a flow imbalance between the two fluids.

Plots of the stream function q and its derivative with respect to Φ_i versus the interface position ϕ are shown for some of the experiments (Figure 4.6 $-$ 4.14). Dimensionless parameters for each experiment are given. The dimensionless shear stress τ versus shear rate γ plots are also shown.

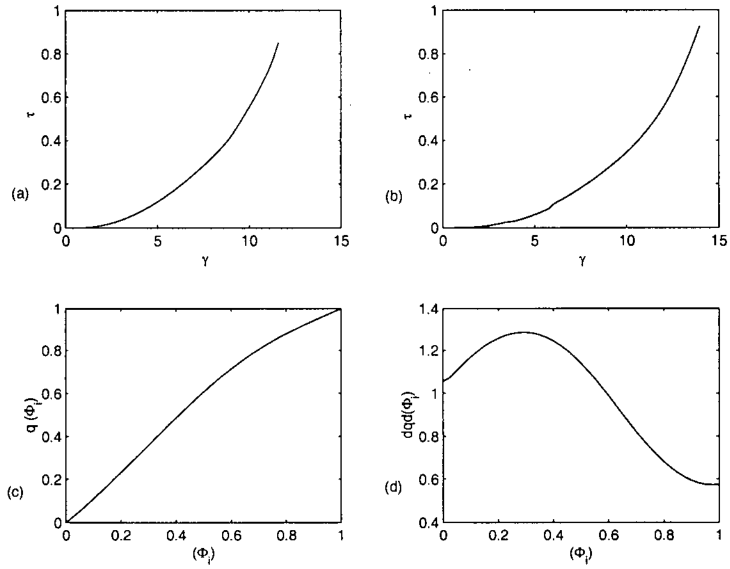

Figure 4.6: Experiment 6 (a): Unsteady displacement ($e = 0.2$; $\rho_m = \rho_c = 1$; $\tau_{m,y} = 0.25$; $\tau_{c,y} = 0.28$; angle of inclination $\beta = 0.26$; Shear stress versus shear rate plots: (a) Mud; (b) Cement.)

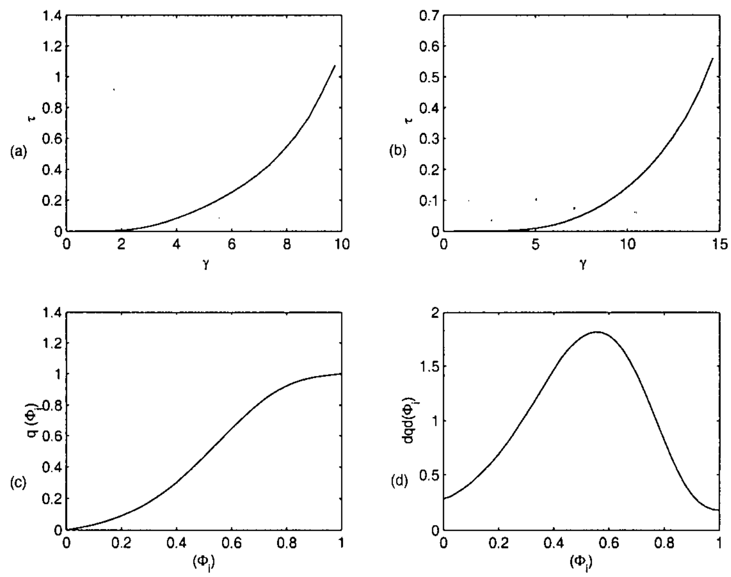

Figure 4.7: Experiment 10 (d): Indeterminate ($e = 0.5$; $\rho_m = \rho_c = 1$; $\tau_{m,y} = 0.25$; $\tau_{c,y} = 0.24$; angle of inclination $\beta = 0.78$; Shear stress versus shear rate plots: (a) Mud; (b) Cement.)

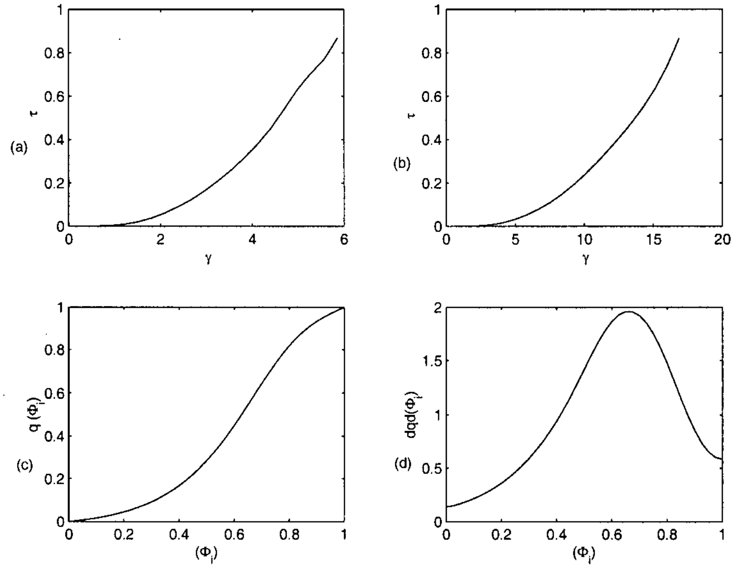

Figure 4.8: Experiment 11 (a): Indeterminate ($e = 0.5$; $\rho_m = \rho_c = 1$; $\tau_{m,y} = 0.2$; $\tau_{c,y} = 0.08$; angle of inclination $\beta = 0.26$; Shear stress versus shear rate plots: (a) Mud; (b) Cement.)

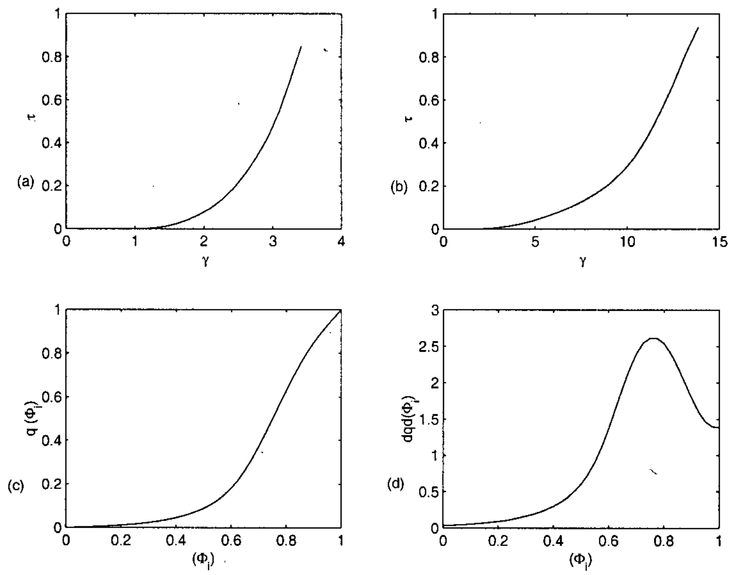

Figure 4.9: Experiment 12 (c): Stable displacement ($e = 0.5$; $\rho_m = \rho_c = 1$; $\tau_{m,y} = 0.07$; $\tau_{c,y} = 1.16$; angle of inclination $\beta = 0.52$; Shear stress versus shear rate plots: (a) Mud; (b) Cement.)

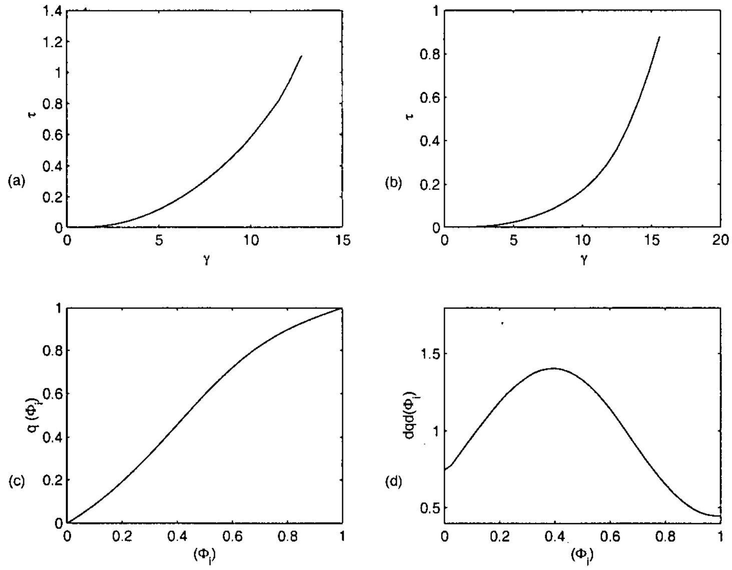

Figure 4.10: Experiment 16 (d): Indeterminate ($e = 0.3$; $\rho_m = 1.11$ $\rho_c = 1.16$; $\tau_{m,y} = 0.5$; $\tau_{c,y} = 0.2$; b=0.005; angle of inclination $\beta = 0.78$; Shear stress versus shear rate plots: (a) Mud; (b) Cement.)

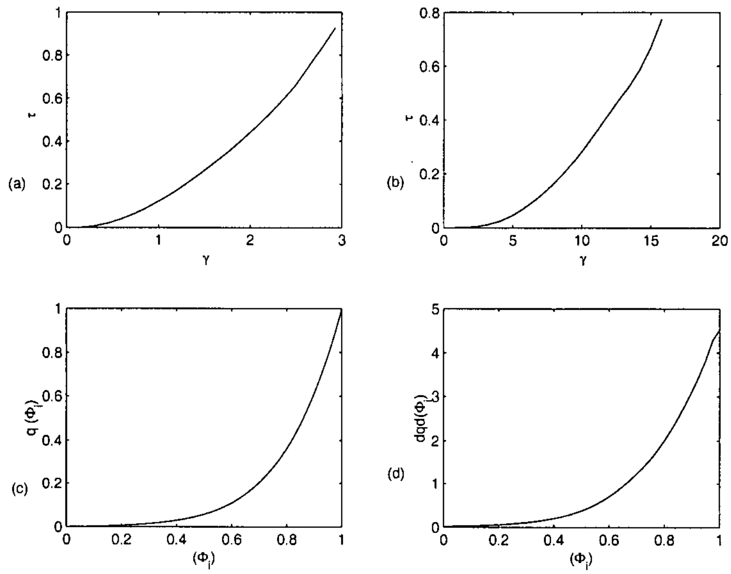

Figure 4.11: Experiment 17 (a): Stable displacement ($e = 0.3$; $\rho_m = 1.08$ $\rho_c = 1.17$; $\tau_{m,y} = 0.1$; $\tau_{c,y} = 0.6$; b=0.032; angle of inclination $\beta = 0.26$; Shear stress versus shear rate plots: (a) Mud; (b) Cement.)

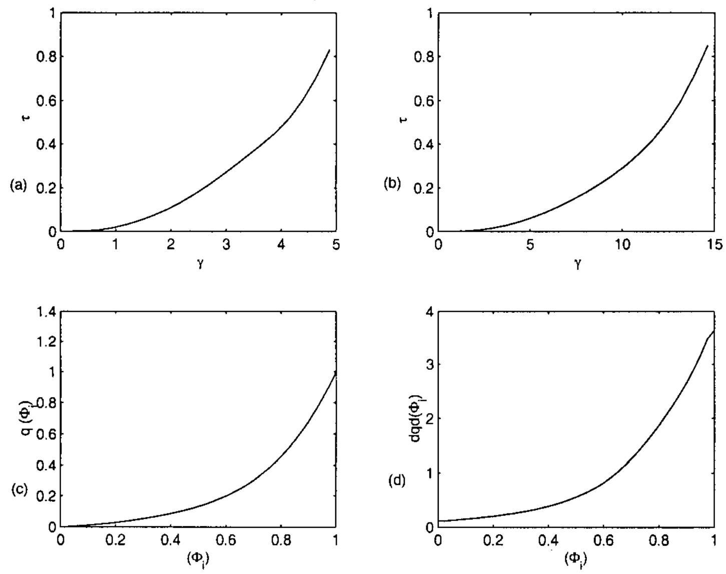

Figure 4.12: Experiment 21 (d): Stable displacement ($e = 0.2$; $\rho_m = 1.08$ $\rho_c = 1.13$; $\tau_{m,y} = 0.07$; $\tau_{c,y} = 0.6$; b=0.006; angle of inclination $\beta = 0.78$; Shear stress versus shear rate plots: (a) Mud; (b) Cement.)

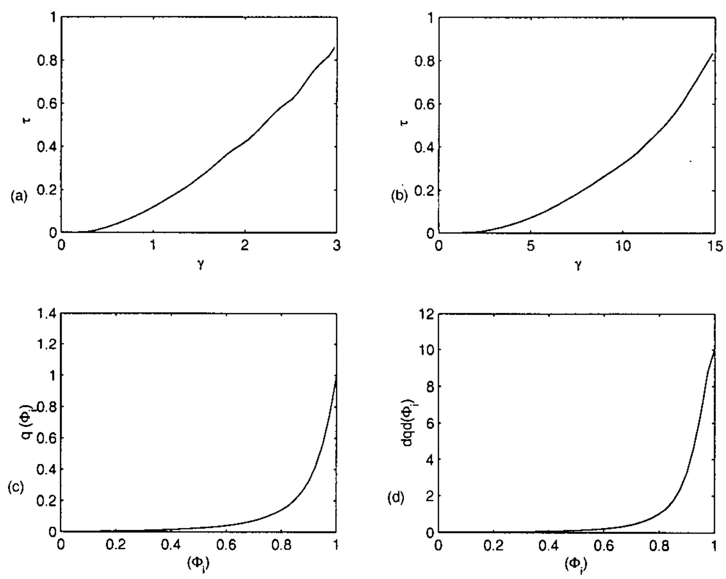

Figure 4.13: Experiment 23 (c): Stable displacement ($e = 0$; $\rho_m = 1.11$ $\rho_c = 1.14$; $\tau_{m,y} = 0.09$; $\tau_{c,y} = 0.24$; b=0.002; angle of inclination $\beta = 0.52$; Shear stress versus shear rate plots: (a) Mud; (b) Cement.)

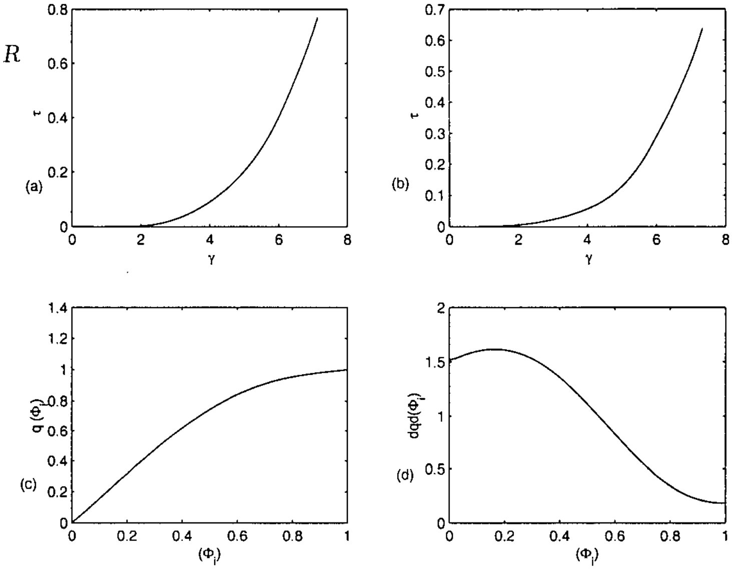

Figure 4.14: Experiment 31 (d): Unsteady displacement ($e = 0.3$; $\rho_m = 1.094$ $\rho_c = 1.201$; $\tau_{m,y} = 0.18$; $\tau_{c,y} = 0.64$; b=0.026; angle of inclination $\beta = 0.78$; Shear stress versus shear rate plots: (a) Mud; (b) Cement.)

4.2 Comparison with the model

The model results compared with the experimental results are presented in the tables $4.1 - 4.5$.

$Exp.$	$Fluid1$	$Fluid2$	$Q(l/min)$	β	e	$\rho_1(kg/m^3)$	$\rho_2(kg/m^3)$	Model	Experiment
$1(a)$	(05/06) $EZ2 - 0.2\%$	(05/06) $940 - 0.2\%$	8.9	15	0	1000	1000	Stable	Flow bypass
$1(b)$	(05/06) $EZ2 - 0.2\%$	(05/06) $940 - 0.2\%$	8.9	20	0	1000	1000	Stable	Flow bypass
$1(c)$	(05/06) $EZ2 - 0.2\%$	(05/06) $940 - 0.2\%$	8.9	30	0	1000	1000	Stable	Flow bypass
$1(d)$	(05/06) $EZ2 - 0.2\%$	(05/06) $940 - 0.2\%$	8.9	45	0	1000	1000	Stable	Flow bypass
$2(a)$	(02/06) $EZ2 - 0.1\%$	(03/06) $EZ2 - 0.2\%$	12	15	0	1000	1000	Stable	Flow bypass
$2(b)$	(02/06) $EZ2 - 0.1\%$	(03/06) $EZ2 - 0.2\%$	12	20	0	1000	1000	Stable	Flow bypass
$2(c)$	(02/06) $EZ2 - 0.1\%$	(03/06) $EZ2 - 0.2\%$	12	30	0	1000	1000	Stable	Flow bypass
$2(d)$	(02/06) $EZ2 - 0.1\%$	(03/06) $EZ2 - 0.2\%$	12	45	0	1000	1000	Stable	Flow bypass
$3(a)$	(30/05) $940 - 0.1\%$	$940 - 0.2\%$	11.2	15	0	1000	1000	Stable	Flow bypass
$3(b)$	(30/05) $940 - 0.1\%$	$940 - 0.2\%$	11.2	20	0	1000	1000	Stable	Flow bypass
$3(c)$	(30/05) $940 - 0.1\%$	$940 - 0.2\%$	11.2	30	0	1000	1000	Stable	Flow bypass
$3(d)$	(30/05) $940 - 0.1\%$	$940 - 0.2\%$	11.2	45	0	1000	1000	Stable	Flow bypass
$4(a)$	(12/06) $EZ2 - 0.2\%$	(12/06) $940 - 0.2\%$	9	15	0.2	1000	1000	Unsteady	Unsteady
$4(b)$	(12/06) $EZ2 - 0.2\%$	(12/06) $940 - 0.2\%$	9	20	0.2	1000	1000	Unsteady	Unsteady
$4(c)$	(12/06) $EZ2 - 0.2\%$	(12/06) $940 - 0.2\%$	9	30	0.2	1000	1000	Unsteady	Unsteady
$4(d)$	(12/06) $EZ2 - 0.2\%$	(12/06) $940 - 0.2\%$	9	45	0.2	1000	1000	Unsteady	Unsteady
$5(a)$	(03/06) $EZ2 - 0.1\%$	(13/06) $EZ2 - 0.2\%$	11.9	15	0.2	1000	1000	Stable	Unsteady
$5(b)$	(03/06) $EZ2 - 0.1\%$	(13/06) $EZ2 - 0.2\%$	11.9	20	0.2	1000	1000	Stable	Unsteady
$5(c)$	(03/06) $EZ2 - 0.1\%$	(13/06) $EZ2 - 0.2\%$	11.9	30	0.2	1000	1000	Stable	Unsteady
$5(d)$	(03/06) $EZ2 - 0.1\%$	(13/06) $EZ2 - 0.2\%$	11.9	45	0.2	1000	1000	Stable	Unsteady
$6(a)$	(10/06) $940 - 0.1\%$	(10/06) $940 - 0.2\%$	10	15	0.2	1000	1000	Unsteady	Unsteady
$6(b)$	(10/06) $940 - 0.1\%$	(10/06) $940 - 0.2\%$	10	20	0.2	1000	1000	Unsteady	Unsteady
$6(c)$	(10/06) $940 - 0.1\%$	(10/06) $940 - 0.2\%$	10	30	0.2	1000	1000	Unsteady	Unsteady
$6(d)$	(10/06) $940 - 0.1\%$	(10/06) $940 - 0.2\%$	10	45	0.2	1000	1000	Unsteady	Unsteady
$7(a)$	(15/06) $EZ2 - 0.2\%$	(13/06) $940 - 0.2\%$	10.9	15	0.3	1000	1000	Stable	Unsteady
$7(b)$	(15/06) $EZ2 - 0.2\%$	(13/06) $940 - 0.2\%$	10.9	20	0.3	1000	1000	Stable	Unsteady
$7(c)$	(15/06) $EZ2 - 0.2\%$	(13/06) $940 - 0.2\%$	10.9	30	0.3	1000	1000	Stable	Unsteady
$7(d)$	(15/06) $EZ2 - 0.2\%$	(13/06) $940 - 0.2\%$	10.9	45	0.3	1000	1000	Unsteady	Unsteady
$8(a)$	(15/06) $EZ2 - 0.1\%$	(16/06) $EZ2 - 0.2\%$	10.1	15	0.3	1000	1000	Unsteady	Unsteady
$8(b)$	(15/06) $EZ2 - 0.1\%$	(16/06) $EZ2 - 0.2\%$	10.1	20	0.3	1000	1000	Unsteady	Unsteady
$8(c)$	(15/06) $EZ2 - 0.1\%$	(16/06) $EZ2 - 0.2\%$	10.1	30	0.3	1000	1000	Unsteady	Unsteady
$8(d)$	(15/06) $EZ2 - 0.1\%$	(16/06) $EZ2 - 0.2\%$	10.1	45	0.3	1000	1000	Unsteady	Unsteady

Table 4.1: Comparison of experiments with the model - experiments 1 - 8.

$Exp.$	$Fluid1$	$Fluid2$	$Q(l/min)$	β	e	$\rho_1(kg/m^3)$	$\rho_2(kg/m^3)$	Model	Experiment
9(a)	(16/06) 940 − 0.1%	(17/06) 940 − 0.2%	10.5	15	0.3	1000	1000	Unsteady	Unsteady
9(b)	(16/06) 940 − 0.1%	(17/06) 940 − 0.2%	10.5	20	0.3	1000	1000	Unsteady	Unsteady
9(c)	(16/06) 940 − 0.1%	(17/06) 940 − 0.2%	10.5	30	0.3	1000	1000	Unsteady	Unsteady
9(d)	(16/06) 940 − 0.1%	(17/06) 940 − 0.2%	10.5	45	0.3	1000	1000	Unsteady	Unsteady
10(a)	(18/06) $EZ2$ − 0.2%	(18/06) 940 − 0.2%	10.3	15	0.5	1000	1000	indeterminate	Unsteady
10(b)	(18/06) $EZ2$ − 0.2%	(18/06) 940 − 0.2%	10.3	20	0.5	1000	1000	indeterminate	Unsteady
10(c)	(18/06) $EZ2$ − 0.2%	(18/06) 940 − 0.2%	10.3	30	0.5	1000	1000	indeterminate	Unsteady
10(d)	(18/06) $EZ2$ − 0.2%	(18/06) 940 − 0.2%	10.3	45	0.5	1000	1000	indeterminate	Unsteady
11(a)	(17/06) $EZ2$ − 0.1%	$EZ2$ − 0.2%	10.8	15	0.5	1000	1000	indeterminate	Unsteady
11(b)	(17/06) $EZ2$ − 0.1%	$EZ2$ − 0.2%	10.8	20	0.5	1000	1000	indeterminate	Unsteady
11(c)	(17/06) $EZ2$ − 0.1%	$EZ2$ − 0.2%	10.8	30	0.5	1000	1000	indeterminate	Unsteady
11(d)	(17/06) $EZ2$ − 0.1%	$EZ2$ − 0.2%	10.8	45	0.5	1000	1000	indeterminate	Unsteady
12(a)	(19/06) 940 − 0.1%	(19/06) 940 − 0.2%	12.9	15	0.5	1000	1000	Stable	Unsteady
12(b)	(19/06) 940 − 0.1%	(19/06) 940 − 0.2%	12.9	20	0.5	1000	1000	Stable	Unsteady
12(c)	(19/06) 940 − 0.1%	(19/06) 940 − 0.2%	12.9	30	0.5	1000	1000	Stable	Unsteady
12(d)	(19/06) 940 − 0.1%	(19/06) 940 − 0.2%	12.9	45	0.5	1000	1000	Stable	Unsteady
13(a)	(22/06) $EZ2$ − 0.2%	(22/06) 940 − 0.2%	11.1	15	0.5	1090	1169	indeterminate	Unsteady
13(b)	(22/06) $EZ2$ − 0.2%	(22/06) 940 − 0.2%	11.1	20	0.5	1090	1169	indeterminate	Unsteady
13(c)	(22/06) $EZ2$ − 0.2%	(22/06) 940 − 0.2%	11.1	30	0.5	1090	1169	indeterminate	Unsteady
13(d)	(22/06) $EZ2$ − 0.2%	(22/06) 940 − 0.2%	11.1	45	0.5	1090	1169	indeterminate	Unsteady
14(a)	(20/06) $EZ2$ − 0.1%	(20/06) $EZ2$ − 0.2%	12.1	15	0.5	1104	1164	Stable	Unsteady
14(b)	(20/06) $EZ2$ − 0.1%	(20/06) $EZ2$ − 0.2%	12.1	20	0.5	1104	1164	Stable	Unsteady
14(c)	(20/06) $EZ2$ − 0.1%	(20/06) $EZ2$ − 0.2%	12.1	30	0.5	1104	1164	Stable	Unsteady
14(d)	(20/06) $EZ2$ − 0.1%	(20/06) $EZ2$ − 0.2%	12.1	45	0.5	1104	1164	Stable	Unsteady
15(a)	(22/06) 940 − 0.1%	(22q/06) 940 − 0.2%	12.7	15	0.5	1096	1158	Stable	Unsteady
15(b)	(22/06) 940 − 0.1%	(22q/06) 940 − 0.2%	12.7	20	0.5	1096	1158	Stable	Unsteady
15(c)	(22/06) 940 − 0.1%	(22q/06) 940 − 0.2%	12.7	30	0.5	1096	1158	Stable	Unsteady
15(d)	(22/06) 940 − 0.1%	(22q/06) 940 − 0.2%	12.7	45	0.5	1096	1158	Stable	Unsteady
16(a)	(24q/06) $EZ2$ − 0.2%	(25/06) 940 − 0.2%	10.5	15	0.3	1106	1156	indeterminate	Flowbypass
16(b)	(24q/06) $EZ2$ − 0.2%	(25/06) 940 − 0.2%	10.5	20	0.3	1106	1156	indeterminate	Flowbypass
16(c)	(24q/06) $EZ2$ − 0.2%	(25/06) 940 − 0.2%	10.5	30	0.3	1106	1156	indeterminate	Flowbypass
16(d)	(24q/06) $EZ2$ − 0.2%	(25/06) 940 − 0.2%	10.5	45	0.3	1106	1156	indeterminate	Flowbypass

Table 4.2: Comparison of experiments with the model - experiments 9 - 16.

Exp.	*Fluid1*	*Fluid2*	$Q(l/min)$	β	e	$\rho_1(kg/m^3)$	$\rho_2(kg/m^3)$	Model	Experiment
17(a)	(23/06) $EZ2 - 0.1\%$	(23/06) $EZ2 - 0.2\%$	11.8	15	0.3	1084	1170	Stable	Unsteady
17(b)	(23/06) $EZ2 - 0.1\%$	(23/06) $EZ2 - 0.2\%$	11.8	20	0.3	1084	1170	Stable	Unsteady
17(c)	(23/06) $EZ2 - 0.1\%$	(23/06) $EZ2 - 0.2\%$	11.8	30	0.3	1084	1170	Stable	Unsteady
17(d)	(23/06) $EZ2 - 0.1\%$	(23/06) $EZ2 - 0.2\%$	11.8	45	0.3	1084	1170	Stable	Unsteady
18(a)	(23/06) 940 − 0.1%	(24/06) 940 − 0.2%	10.9	15	0.3	1110	1144	Stable	Unsteady
18(b)	(23/06) 940 − 0.1%	(24/06) 940 − 0.2%	10.9	20	0.3	1110	1144	Stable	Unsteady
18(c)	(23/06) 940 − 0.1%	(24/06) 940 − 0.2%	10.9	30	0.3	1110	1144	Stable	Unsteady
18(d)	(23/06) 940 − 0.1%	(24/06) 940 − 0.2%	10.9	45	0.3	1110	1144	Stable	Unsteady
19(a)	(25/06) $EZ2 - 0.2\%$	(26/06) 940 − 0.2%	8.9	15	0.2	1076	1132	indeterminate	Unsteady
19(b)	(25/06) $EZ2 - 0.2\%$	(26/06) 940 − 0.2%	8.9	20	0.2	1076	1132	indeterminate	Unsteady
19(c	(25/06) $EZ2 - 0.2\%$	(26/06) 940 − 0.2%	8.9	30	0.2	1076	1132	indeterminate	Unsteady
19(d)	(25/06) $EZ2 - 0.2\%$	(26/06) 940 − 0.2%	8.9	45	0.2	1076	1132	indeterminate	Unsteady
20(a)	(24/06) $EZ2 - 0.1\%$	(24/06) $EZ2 - 0.2\%$	10.6	15	0.2	1108	1160	Stable	Unsteady
20(b)	(24/06) $EZ2 - 0.1\%$	(24/06) $EZ2 - 0.2\%$	10.6	20	0.2	1108	1160	Stable	Unsteady
20(c	(24/06) $EZ2 - 0.1\%$	(24/06) $EZ2 - 0.2\%$	10.6	30	0.2	1108	1160	Stable	Unsteady
20(d)	(24/06) $EZ2 - 0.1\%$	(24/06) $EZ2 - 0.2\%$	10.6	45	0.2	1108	1160	Stable	Unsteady
21(a)	(25/06) 940 − 0.1%	(26q/06) 940 − 0.2%	13.4	15	0.2	1082	1136	Stable	Unsteady
21(b)	(25/06) 940 − 0.1%	(26q/06) 940 − 0.2%	13.4	20	0.2	1082	1136	Stable	Unsteady
21(c)	(25/06) 940 − 0.1%	(26q/06) 940 − 0.2%	13.4	30	0.2	1082	1136	Stable	Unsteady
21(d)	(25/06) 940 − 0.1%	(26q/06) 940 − 0.2%	13.4	45	0.2	1082	1136	Stable	Unsteady
22(a)	(03/07) $EZ2 - 0.2\%$	(03/07) 940 − 0.2%	10.9	15	0	1088	1136	Stable	Flowbypass
22(b)	(03/07) $EZ2 - 0.2\%$	(03/07) 940 − 0.2%	10.9	30	0	1088	1136	Stable	Flowbypass
22(c)	(03/07) $EZ2 - 0.2\%$	(03/07) 940 − 0.2%	10.9	30	0	1088	1136	Stable	Flowbypass
22(d)	(03/07) $EZ2 - 0.2\%$	(03/07) 940 − 0.2%	10.9	45	0	1088	1136	Stable	Flowbypass
23(a)	(04/07) $EZ2 - 0.1\%$	(04/07) $EZ2 - 0.2\%$	12	15	0	1110	1138	Stable	Stable
23(b)	(04/07) $EZ2 - 0.1\%$	(04/07) $EZ2 - 0.2\%$	12	20	0	1110	1138	Stable	Stable
23(c)	(04/07) $EZ2 - 0.1\%$	(04/07) $EZ2 - 0.2\%$	12	30	0	1110	1138	Stable	Stable
23(d)	(04/07) $EZ2 - 0.1\%$	(04/07) $EZ2 - 0.2\%$	12	45	0	1110	1138	Stable	Stable
24(a)	(04/07) 940 − 0.1%	(03q/07) 940 − 0.2%	12.5	15	0	1084	1158	Stable	Stable
24(b)	(04/07) 940 − 0.1%	(03q/07) 940 − 0.2%	12.5	20	0	1084	1158	Stable	Stable
24(c)	(04/07) 940 − 0.1%	(03q/07) 940 − 0.2%	12.5	30	0	1084	1158	Stable	Stable
24(d)	(04/07) 940 − 0.1%	(03q/07) 940 − 0.2%	12.5	45	0	1084	1158	Stable	Stable

Table 4.3: Comparison of experiments with the model - experiments 17 - 24.

$Exp.$	$Fluid1$	$Fluid2$	$Q(l/min)$	β	e	$\rho_1(kg/m^3)$	$\rho_2(kg/m^3)$	Model	Experiment
$25(a)$	(05/07) $EZ2 - 0.2\%$	(06/07) $940 - 0.2\%$	11.9	15	0	1089	1201	Stable	Stable
$25(b)$	(05/07) $EZ2 - 0.2\%$	(06/07) $940 - 0.2\%$	11.9	20	0	1089	1201	Stable	Stable
$25(c)$	(05/07) $EZ2 - 0.2\%$	(06/07) $940 - 0.2\%$	11.9	30	0	1089	1201	Stable	Stable
$25(d)$	(05/07) $EZ2 - 0.2\%$	(06/07) $940 - 0.2\%$	11.9	45	0	1089	1201	Stable	Stable
$26(a)$	(06/07) $EZ2 - 0.1\%$	(07/07) $EZ2 - 0.2\%$	12.5	15	0	1106	1185	Stable	Stable
$26(b)$	(06/07) $EZ2 - 0.1\%$	(07/07) $EZ2 - 0.2\%$	12.5	20	0	1106	1185	Stable	Stable
$26(c)$	(06/07) $EZ2 - 0.1\%$	(07/07) $EZ2 - 0.2\%$	12.5	30	0	1106	1185	Stable	Stable
$26(d)$	(06/07) $EZ2 - 0.1\%$	(07/07) $EZ2 - 0.2\%$	12.5	45	0	1106	1185	Stable	Stable
$27(a)$	(07/07) $940 - 0.1\%$	(07/07) $940 - 0.2\%$	13.3	15	0	1093	1236	Stable	Stable
$27(b)$	(07/07) $940 - 0.1\%$	(07/07) $940 - 0.2\%$	13.3	20	0	1093	1236	Stable	Stable
$27(c)$	(07/07) $940 - 0.1\%$	(07/07) $940 - 0.2\%$	13.3	30	0	1093	1236	Stable	Stable
$27(d)$	(07/07) $940 - 0.1\%$	(07/07) $940 - 0.2\%$	13.3	45	0	1093	1236	Stable	Stable
$28(a)$	(08/07) $EZ2 - 0.2\%$	(08/07) $940 - 0.2\%$	11	15	0.2	1084	1177	Stable	Flowbypass
$28(b)$	(08/07) $EZ2 - 0.2\%$	(08/07) $940 - 0.2\%$	11	20	0.2	1084	1177	Stable	Flowbypass
$28(c)$	(08/07) $EZ2 - 0.2\%$	(08/07) $940 - 0.2\%$	11	30	0.2	1084	1177	Stable	Flowbypass
$28(d)$	(08/07) $EZ2 - 0.2\%$	(08/07) $940 - 0.2\%$	11	45	0.2	1084	1177	Stable	Flowbypass
$29(a)$	(09/07) $EZ2 - 0.1\%$	(10/07) $EZ2 - 0.2\%$	10.9	15	0.2	1097	1168	Stable	Stable
$29(b)$	(09/07) $EZ2 - 0.1\%$	(10/07) $EZ2 - 0.2\%$	10.9	20	0.2	1097	1168	Stable	Stable
$29(c)$	(09/07) $EZ2 - 0.1\%$	(10/07) $EZ2 - 0.2\%$	10.9	30	0.2	1097	1168	Stable	Stable
$29(d)$	(09/07) $EZ2 - 0.1\%$	(10/07) $EZ2 - 0.2\%$	10.9	45	0.2	1097	1168	Stable	Stable
$30(a)$	(09/07) $940 - 0.1\%$	(10/07) $940 - 0.2\%$	10.1	15	0.2	1077	1225	Stable	Stable
$30(b)$	(09/07) $940 - 0.1\%$	(10/07) $940 - 0.2\%$	10.1	20	0.2	1077	1225	Stable	Stable
$30(c)$	(09/07) $940 - 0.1\%$	(10/07) $940 - 0.2\%$	10.1	30	0.2	1077	1225	Stable	Stable
$30(d)$	(09/07) $940 - 0.1\%$	(10/07) $940 - 0.2\%$	10.1	45	0.2	1077	1225	Stable	Stable
$31(a)$	(10/07) $EZ2 - 0.2\%$	(10/07) $940 - 0.2\%$	12.9	15	0.3	1094	1201	Unsteady	Unsteady
$31(b)$	(10/07) $EZ2 - 0.2\%$	(10/07) $940 - 0.2\%$	12.9	20	0.3	1094	1201	Unsteady	Unsteady
$31(c)$	(10/07) $EZ2 - 0.2\%$	(10/07) $940 - 0.2\%$	12.9	30	0.3	1094	1201	Unsteady	Unsteady
$31(d)$	(10/07) $EZ2 - 0.2\%$	(10/07) $940 - 0.2\%$	12.9	45	0.3	1094	1201	Unsteady	Unsteady
$32(a)$	(11/07) $EZ2 - 0.1\%$	(11/07) $EZ2 - 0.2\%$	11.5	15	0.3	1093	1176	Stable	Unsteady
$32(b)$	(11/07) $EZ2 - 0.1\%$	(11/07) $EZ2 - 0.2\%$	11.5	20	0.3	1093	1176	Stable	Unsteady
$32(c)$	(11/07) $EZ2 - 0.1\%$	(11/07) $EZ2 - 0.2\%$	11.5	30	0.3	1093	1176	Stable	Unsteady
$32(d)$	(11/07) $EZ2 - 0.1\%$	(11/07) $EZ2 - 0.2\%$	11.5	45	0.3	1093	1176	Stable	Unsteady

Table 4.4: Comparison of experiments with the model - experiments 25 - 32.

$Exp.$	$Fluid1$	$Fluid2$	$Q(l/min)$	β	e	$\rho_1(kg/m^3)$	$\rho_2(kg/m^3)$	Model	Experiment
$33(a)$	(11/07) $940 - 0.1\%$	(11/07) $940 - 0.2\%$	11.8	15	0.3	1096	1172	Stable	Unsteady
$33(b)$	(11/07) $940 - 0.1\%$	(11/07) $940 - 0.2\%$	11.8	20	0.3	1096	1172	Stable	Unsteady
$33(c)$	(11/07) $940 - 0.1\%$	(11/07) $940 - 0.2\%$	11.8	30	0.3	1096	1172	Stable	Unsteady
$33(d)$	(11/07) $940 - 0.1\%$	(11/07) $940 - 0.2\%$	11.8	45	0.3	1096	1172	Stable	Unsteady
$34(a)$	(13/07) $EZ2 - 0.2\%$	(14/07) $940 - 0.2\%$	13.6	15	0.5	1072	1170	indeterminate	Unsteady
$34(b)$	(13/07) $EZ2 - 0.2\%$	(14/07) $940 - 0.2\%$	13.6	20	0.5	1072	1170	indeterminate	Unsteady
$34(c)$	(13/07) $EZ2 - 0.2\%$	(14/07) $940 - 0.2\%$	13.6	30	0.5	1072	1170	indeterminate	Unsteady
$34(d)$	(13/07) $EZ2 - 0.2\%$	(14/07) $940 - 0.2\%$	13.6	45	0.5	1072	1170	indeterminate	Unsteady
$35(a)$	(13/07) $EZ2 - 0.1\%$	(14/07) $EZ2 - 0.2\%$	13	15	0.5	1110	1175	Stable	Unsteady
$35(b)$	(13/07) $EZ2 - 0.1\%$	(14/07) $EZ2 - 0.2\%$	13	20	0.5	1110	1175	Stable	Unsteady
$35(c)$	(13/07) $EZ2 - 0.1\%$	(14/07) $EZ2 - 0.2\%$	13	30	0.5	1110	1175	Stable	Unsteady
$35(d)$	(13/07) $EZ2 - 0.1\%$	(14/07) $EZ2 - 0.2\%$	13	45	0.5	1110	1175	Stable	Unsteady
$36(a)$	(12/07) $940 - 0.1\%$	(12/07) $940 - 0.2\%$	16.6	15	0.5	1106	1184	Stable	Unsteady
$36(b)$	(12/07) $940 - 0.1\%$	(12/07) $940 - 0.2\%$	16.6	20	0.5	1106	1184	Stable	Unsteady
$36(c)$	(12/07) $940 - 0.1\%$	(12/07) $940 - 0.2\%$	16.6	30	0.5	1106	1184	Stable	Unsteady
$36(d)$	(12/07) $940 - 0.1\%$	(12/07) $940 - 0.2\%$	16.6	45	0.5	1106	1184	Stable	Unsteady

Table 4.5: Comparison of experiments with the model - experiments 33 - 36.

Chapter 5
Discussion, Conclusions and Recommendations

5.1 Discussion

In this thesis, we have investigated the effects of eccentricity, rheology, inclination and density contrast on laminar displacement of two fluids in a vertical annulus experimentally. We have compared our experimental findings with a model of non-Newtonian displacement flow in annular geometry. Although extensive work has been done in this area previously, [1, 2, 3, 4, 5, 6, 7, 8, 9, 12, 17] we report some new interesting results of importance.

1. Concentric, isodensity, inclinations ($15°, 20°, 30°, 45°$), more viscous fluid displacing less viscous fluid, flow rate $8 - 11.2 l/min$: Our experiments show that Flow bypass occurs in concentric annulus when there is no density contrast between the fluids. It is observed in some cases for a density contrast of 5% but does not exist for a 10% density contrast between the two fluids. This happens at all inclinations. Positive rheology difference between the two fluids does not prevent its formation. The model predicts a stable displacement for all cases for a concentric annulus.

2. e = 0.2, isodensity, inclinations ($15°, 20°, 30°, 45°$), more viscous fluid displacing less viscous fluid, flow rates $9 - 11.9 l/min$: Our experiments show that the displacement is unsteady. The model predicts both unsteady and stable displacement. The displacement is stable when the flow rate is increased to 11.9l/min. For lower flow rates, $9 - 10 l/min$, the displacement is unsteady.

3. e = 0.3, isodensity, inclinations ($15^\circ, 20^\circ, 30^\circ, 45^\circ$), more viscous fluid displacing less viscous fluid, flow rate $10 - 10.9l/min$: Our experiments show that the displacement is unsteady. The model predicts stable displacement at a flow rate of $10.9l/min$ and unsteady at lower flow rates ($10.1 - 10.5l/min$).

4. e = 0.5, isodensity, inclinations ($15^\circ, 20^\circ, 30^\circ, 45^\circ$), more viscous fluid displacing less viscous fluid, flow rate $10.3 - 12.9l/min$: Our experiments show that the displacement is unsteady. The model predicts indeterminate displacement for lower flow rates ($10.3 - 10.8l/min$) and stable displacement at higher flow rates ($12.9l/min$).

5. e = 0, 5% density contrast, inclinations ($15^\circ, 20^\circ, 30^\circ, 45^\circ$), more viscous fluid displacing less viscous fluid, flow rate $10.9 - 12.5l/min$: Our experiments show that flow bypass occurs at lower flow rates ($10.9l/min$). The displacement is stable at higher flow rates ($12 - 12.5l/min$).

6. e = 0.2, 5% density contrast, inclinations ($15^\circ, 20^\circ, 30^\circ, 45^\circ$), more viscous fluid displacing less viscous fluid, flow rate $8.9 - 13.4l/min$: Our experiments show that displacement is unsteady. The model predicts indeterminate displacement at lower flow rates ($8.9l/min$) and stable displacement at higher flow rates ($10.6 - 13.4l/min$).

7. e = 0.3, 5% density contrast, inclinations ($15^\circ, 20^\circ, 30^\circ, 45^\circ$), more viscous fluid displacing less viscous fluid, flow rate $10.5 - 11.8l/min$: Our experiments show that flow bypass occurs at lower flow rates ($10.5l/min$). The displacement is unsteady at higher flow rates ($10.9 - 11.8l/min$). The model predicts indeterminate displacement at lower flow rates ($10.5l/min$) and unsteady displacement at higher flow rates ($10.9 - 11.8l/min$).

8. e = 0.5, 5% density contrast, inclinations ($15^\circ, 20^\circ, 30^\circ, 45^\circ$), more viscous fluid displacing less viscous fluid, flow rate $11.1 - 12.7l/min$: Our experiments show that the displacement is unsteady. The model predicts indeterminate displacement at lower flow rates ($11.1l/min$) and stable displacement at higher flow rates ($12.1 - 12.7l/min$).

9. e = 0, 10% density contrast, inclinations ($15°, 20°, 30°, 45°$), more viscous fluid displacing less viscous fluid, flow rate $11.9 - 13.3l/min$: Our experiments show that the displacement is stable. The model predicts stable displacement. The model is in good agreement with the experiments.

10. e = 0.2, 10% density contrast, inclinations ($15°, 20°, 30°, 45°$), more viscous fluid displacing less viscous fluid, flow rate $10.1 - 11l/min$: Our experiments show that the displacement is stable at lower flow rates ($10.1 - 10.9l/min$) and flow bypass occurs at higher flow rates ($11l/min$). The model predicts stable displacement.

11. e = 0.3, 10% density contrast, inclinations ($15°, 20°, 30°, 45°$), more viscous fluid displacing less viscous fluid, flow rate $11.5 - 12.9l/min$: Our experiments show that the displacement is unsteady. The model predicts stable displacement at lower flow rates ($11.5 - 11.8l/min$) and unsteady displacement at higher flow rates ($12.9l/min$).

12. e = 0.5, 10% density contrast, inclinations ($15°, 20°, 30°, 45°$), more viscous fluid displacing less viscous fluid, flow rate $13.6 - 16.6l/min$: Our experiments show that the displacement is unsteady. The model predicts stable displacement at higher flow rates ($16.6l/min$) and indeterminate displacement at lower flow rates ($13.6l/min$).

5.2 Conclusions

1. Minimum displacement occurs at an $e = 0.5$.

2. Inclination reduces displacement efficiency in an annulus. The effect becomes more significant for inclinations above 30 degrees from the vertical.

3. Higher flow rates ($13.6 - 16.6l/min$) improve displacement.

4. Higher positive density contrast (10%) improve displacement in both concentric and eccentric annulus.

5. Flow bypass occurs in a concentric annulus for lower density contrasts (5%). It can be avoided by having a higher density contrast (10%) between the two fluids. Higher flow

rates ($1316 l/min$) can help avoid flow bypass in an eccentric annulus ($e = 0.2, e = 0.3$).

5.3 Recommendations for future work

For future work in the laboratory, following guidelines are given for near - vertical oil wells:

1. The cause of flow bypass is unclear. Tests should be conducted on a much smaller apparatus, for example: a 2 m annular tube could be used for running the tests. The cause of flow bypass should be analyzed and then the experiments should be conducted on the annular flow loop used for our experiments.

2. Quantitative analysis of the experimental results should be done. A method should be devised to measure the interface velocity. Photo detector sensors could be used to measure the interface velocity.

3. The camera system should be mounted on the end of the annulus in such a way that its easier to record displacement at different inclinations. This should be evident when the videos are recorded.

4. The limits of stable or unsteady displacements should be analyzed by varying the effects of rheology and density contrast between the two fluids.

Bibliography

[1] D.Guillot, D. Hendriks, F. Callet and B. Vidick. Well Cementing, chapter Mud Removal(Chapter 5). *Schlumberger Educational Services, Houston*, 1990.

[2] R.H. McLean, C.W. Manry and W.W.Whitaker. Displacement mechanics in primary cementing. *Society of Petroleum Engineers.*, paper number SPE 1488, 1966.

[3] R.C. Haut and R.C.Crook. Primary Cementing:The noncirculatable mud displacement process. *Society of Petroleum Engineers*, paper number SPE 8253, 1979.

[4] R.C. Haut and R.C.Crook. Primary Cementing:Optimizing for maximum displacement. *World Oil,* pages 105–116, September 1980.

[5] A. Jamot. Displacement de la boue par le latier de ciment dans l'espace annulaire tubageparoi d'un puits. *Revue Assoc.Franc. Techn. Petr.,* 224 pages 27–37, 1974.

[6] C.F. Lockyear and A.P. Hibbert. Integrated primary cementing study defines key factors for field success. *Journal of Petroleum Technology,* pages 1320–1325, December 1989.

[7] C.F. Lockyear, D.F. Ryan and D.F. Gunningham. Cement Channeling: How to predict and prevent. *Society of Petroleum Engineers,* paper number SPE 19865, 1989.

[8] M.Couturier, D. Guillot, H. Hendriks and F. Callet. Design rules and associated spacer properties for optimal mud removal in eccentric annuli. *Society of Petroleum Engineers,* paper number SPE 179, 1987.

[9] I.A. Frigaard Well bore fluid-fluid displacement . *Research and engineering review, RD report 97-020, Confidential report.*, December 1997.

[10] S. Brady, P.P Drecq, K.C. Baker and D.J. Guillot Recent technological advances help solve cement placement problems in Gulf of Mexico. *Society of Petroleum Engineers,* paper number IADC SPE 23927, 1992.

[11] V.C. Kellessidis, R. rafferty, A. Merlo and R. Maglione. Simulator models u-tubing to improve primary cementing. *Oil and Gas Journal,* March 1994.

[12] I.A. Frigaard, S.H. Bittleston and J. Ferguson. Mud removal and cement placement during primary cementing of an oil well. *Journal of Engineering Mathematics,* 43, pages 229–253, 2002.

[13] S.Pelipenko. Displacement of non-Newtonian fluids in an eccentric annulus. *MSc, UBC* , January 2002.

[14] N.R. Young. Design and Construction of an annular flow loop for fluid- fluid displacements. *M.Eng.,* April 2002.

[15] A. Lindner,P. Coussot and D. Bonn. Viscous fingering in a yield stress fluid. *Physical Review Letters,* 85, pages 314–317, 2000

[16] P. Coussot. Saffman-taylor instability in yield stress fluids. *Journal of Fluid Mech.,* 380, pages 363–376, 1999.

[17] M.A. Tehrani and J. Ferguson Non-newtonian displacement in an eccentric annulus. *SCR/SR/017/018/019/FLM/C, Confidential Reports.,* 1992

[18] S.Pelipenko and I.A.Frigaard Visco-plastic fluid displacements in near-vertical narrow eccentric annuli. Part 1: lubriation modelling *Journal of Fluid Mech, Under review,* September 2003

[19] A. Tehrani, J. Ferguson and S.H. Bittleson Laminar displacement in annuli: A combined experimental and theoritcal study. *Society of Petroleum Engineers,* paper number SPE 24569, 1992.